

1 What induced the exceptional 2005 convection event

2 in the northwestern Mediterranean basin?

3 Answers from a modeling study

4 Marine Herrmann,¹ Florence Sevault,¹ Jonathan Beuvier,^{1,2} and Samuel Somot¹

5 Received 1 February 2010; revised 7 October 2010; accepted 15 October 2010; published XX Month 2010.

6 [1] Open-sea convection occurring in the northwestern Mediterranean basin (NWMED) is
 7 at the origin of the formation of Western Mediterranean Deep Water (WMDW), one of
 8 the main Mediterranean water masses. During winter 2004–2005, a spectacular convection
 9 event occurred, observed by several experimental oceanographers. It was associated
 10 with an exceptionally large convection area and unusually warm and salty WMDW.
 11 Explanations were proposed tentatively, relating the unusual characteristics of this event
 12 to the Eastern Mediterranean Transient (EMT) or to the atmospheric conditions during
 13 winter 2004–2005 in the NWMED. They could, however, not be supported until now.
 14 Here we used numerical modeling to understand what drove this convection event.
 15 The control simulation performed for the period 1961–2006 reproduces correctly the
 16 long-term evolution of the Mediterranean Sea circulation, the EMT, and the NWMED
 17 convection event of 2004–2005. Sensitivity simulations are then performed to assess
 18 the respective contributions of atmospheric and oceanic conditions to this event. The
 19 weakness of the winter buoyancy loss since 1988 in the NWMED prevented strong
 20 convection to occur during the 1990s, enabling heat and salt contents to increase in this
 21 region. This resulted in the change of WMDW characteristics observed in 2005. The
 22 strong buoyancy loss of winter 2004–2005 was responsible for the intensity of the
 23 convection observed this winter in terms of depth and volume of newly formed WMDW.
 24 The EMT did not fundamentally modify the convection process but potentially doubled
 25 this volume by inducing a deepening of the heat and salt maximum that weakened the
 26 preconvection stratification.

27 **Citation:** Herrmann, M., F. Sevault, J. Beuvier, and S. Somot (2010), What induced the exceptional 2005 convection event in
 28 the northwestern Mediterranean basin? Answers from a modeling study, *J. Geophys. Res.*, 115, XXXXXX,
 29 doi:10.1029/2010JC006162.

30 1. Introduction

31 [2] Open-sea deep convection takes place in a few regions
 32 of the world, among which the northwestern Mediterranean
 33 basin (NWMED) [Marshall and Schott, 1999]. In this region,
 34 strong winter surface buoyancy loss associated with northern
 35 wind events (Mistral, Tramontane) induce deep convection
 36 events, at the origin of the formation of Western Mediter-
 37 ranean Deep Water (WMDW). During winter 2004–2005, an
 38 exceptionally strong convection event was observed by
 39 several experimental oceanographers [López-Jurado *et al.*,
 40 2005; Salat *et al.*, 2006; Schröder *et al.*, 2006; Font *et al.*,
 41 2007; Schroeder *et al.*, 2008; Smith *et al.*, 2008]: convection
 42 reached the bottom and covered an area much larger than
 43 usually, and WMDW formed this winter was significantly
 44 saltier and warmer than the values reported in the literature
 45 (Table 1). Two major explanations for the exceptional

characteristics of this convection event (intensity and 46
 WMDW characteristics) were proposed by those authors. 47

[3] First, winter 2004–2005 was one of the coldest and 48
 driest winters of the last 40 years [López-Jurado *et al.*, 49
 2005; Font *et al.*, 2007], thus associated with strong sur- 50
 face heat, water and buoyancy losses. The formation of 51
 dense water at the surface being triggered by the buoyancy 52
 loss, those atmospheric conditions certainly played a role in 53
 the intensity of the deep convection event. Moreover, the 54
 strong water loss must have induced an increase of the 55
 surface salinity which could partly explain the larger salinity 56
 of WMDW formed this year. 57

[4] Second, López-Jurado *et al.* [2005] suggested that the 58
 unusual characteristics of the 2005 convection event could 59
 be due to an alteration of the water masses advected into the 60
 convection area. Millot [2005] also proposed that some 61
 observed changes in the Western Mediterranean Deep Water 62
 masses could be due to the presence of modified eastern 63
 waters brought to the Western basin after the Eastern 64
 Mediterranean Transient (EMT, corresponding to the shift 65
 of production of Eastern Mediterranean Deep Water from 66
 the Adriatic to the Aegean subbasins at the beginning of the 67

¹CNRM-GAME, Météo-France/CNRS, Toulouse, France.

²ENSTA-ParisTech/UME, Palaiseau, France.

tl.1 **Table 1.** Observed Characteristics of the Old WMDW (Formed Before 2005) and New WMDW (Formed in 2005)^a

tl.2	Authors	Old DW			New DW		
		T_{DW} (°C)	S_{DW}	ρ_{DW} (kg m ⁻³)	T_{DW} (°C)	S_{DW}	ρ_{DW} (kg m ⁻³)
tl.4	<i>Mertens and Schott</i> [1998]	12.75–12.92	38.41–38.46	29.09–29.10			
tl.5	<i>López-Jurado et al.</i> [2005]	12.83–12.85	38.44–38.46		12.88	38.48–38.49	
tl.6	<i>Schröder et al.</i> [2006]	12.8–12.85	38.44–38.46		12.87–12.90	38.47–38.48	
tl.7	<i>Salat et al.</i> [2006]	12.75–12.82	38.43–38.47	29.115–29.120	12.87–12.90	38.49–38.50	29.130
tl.8	<i>Font et al.</i> [2007]	12.8–12.9	38.43–38.46	29.09–29.10	12.88	38.48	29.117
tl.9	<i>Smith et al.</i> [2008]	12.86	38.46	29.108	12.89	38.48	29.113
tl.10	This study:CTRL, 2005	12.73–12.80	38.423–38.44	>29.10	12.90	38.483	29.116

tl.11 ^aThe values obtained in CTRL from the temperature-salinity diagram shown in Figure 7a are also indicated, with old WMDW corresponding to water
 tl.12 denser than 29.10 kg m⁻³ present in LION on 1 December 2004 and new WMDW corresponding to the densest water formed on 10 March 2005. T_{DW} ,
 tl.13 temperature; S_{DW} , salinity; ρ_{DW} , density.

68 1990s; see *Roether et al.* [2007] for a detailed description of
 69 the EMT). *Gasparini et al.* [2005] indeed showed that the
 70 EMT induced an increase of the density of the eastern
 71 waters flowing westward through the Sicily channel asso-
 72 ciated with a remarkable injection of heat and salt in
 73 the deep Tyrrhenian subbasin. Consequently, *López-Jurado*
 74 *et al.* [2005], *Schröder et al.* [2006] and *Schroeder et al.*
 75 [2008] suggested that the EMT induced the warming and
 76 salting of the intermediate and deep layer of the NWMD.
 77 Being mixed with the rest of the water column when deep
 78 convection occurs, this layer participates in the composition
 79 of WMDW. This could thus explain the warming and salting
 80 of WMDW formed in 2005. Moreover, it could have
 81 induced a modification of the water column structure, hence
 82 of the stratification, which could have impacted the exten-
 83 sion of the deep convection volume.

84 [5] Until now, those explanations were proposed tenta-
 85 tively, but have not been supported yet. In particular, the
 86 relative contributions of the atmospheric and oceanic con-
 87 ditions to the characteristics of the 2005 deep convection
 88 event still need to be clearly quantified. Observations were
 89 indeed very useful to characterize this event, but they do not
 90 provide sufficiently continuous spatial and temporal cover-
 91 age to answer to those questions. Realistic numerical
 92 modeling can help to apprehend the 4-D evolution of the sea
 93 and therefore help to interpret and understand observations.
 94 To our knowledge, however, no realistic oceanic simulation
 95 of the NWMD circulation in 2004–2005 has been per-
 96 formed until now: *Herrmann et al.* [2009] presented a
 97 simulation that was carried out for the 1998–2007 period,
 98 but it did not reproduced the change of WMDW char-
 99 acteristics observed in 2005. In this context, our goal is to
 100 perform realistic numerical modeling of the NWMD 2005
 101 convection event but also of the long-term Mediterranean
 102 circulation before 2004, in order to understand precisely
 103 what triggered this event, and to quantify the contribution of
 104 the different factors involved.

105 [6] We present the numerical model and the simulations
 106 in section 2. Results are then presented and discussed in
 107 section 3. We first examine the long-term evolution of the
 108 water column until 2004 in the NWMD and the influence
 109 of the EMT on the NWMD oceanic conditions. We then
 110 show that the model is able to represent realistically the
 111 2004–2005 NWMD convection event. Finally, we deter-
 112 mine which factors were responsible for the exceptional
 113 characteristics of this event. For that, we assess the influence
 114 of the oceanic and atmospheric conditions before and during
 115 winter 2004–2005. Conclusion and future works are pre-

sented in section 4. Note that in the following, all the values
 given for temperature and density correspond to potential
 temperature and density.

2. Tools and Methods

2.1. Numerical Model

[7] We use the NEMOMED8 model, a Mediterranean
 version of the NEMO numerical ocean model [*Madec*, 2008]
 used and described by *Beuvier et al.* [2010] and *Sevault et al.*
 [2009]. It is an updated version of the model used by *Somot*
et al. [2006] and *Herrmann et al.* [2008] to study the
 NWMD deep convection. NEMOMED8 covers the whole
 Mediterranean Sea plus a buffer zone including a part of the
 near Atlantic Ocean (see Figure 1). The horizontal resolution
 is $1/8^\circ \times 1/8^\circ \cos(\phi)$, with ϕ the latitude, equivalent to a range
 of 9 to 12 km from the north to the south of the Mediterranean
 domain. The grid is tilted and stretched at the Gibraltar Strait
 in order to better follow the SW-NE axis of the real strait
 and to increase the local resolution up to 6 km. The Gibraltar
 Strait is represented with a two-grid point wide strait.
 NEMOMED8 has 43 vertical Z levels with an inhomoge-
 neous distribution (from Z = 6 m at the surface to Z = 200 m at
 the bottom with 25 levels in the first 1000 m). The bathymetry
 is based on the ETOPO 5' × 5' database [*Smith and Sandwell*,
 1997]. A time step of 20 min is applied. NEMOMED8 has a
 filtered free-surface and partial-cell parametrization. The
 horizontal eddy diffusivity is fixed to 125 m² s⁻¹ for the
 tracers (temperature, salinity) using a Laplacian operator and
 the horizontal viscosity coefficients is fixed to $-1.0 \cdot 10^{10}$ m²
 s⁻² for the dynamics (velocity) using a biharmonic operator.
 A 1.5 turbulent closure scheme is used for the vertical eddy
 diffusivity [*Blanke and Delecluse*, 1993] with an enhance-
 ment of the vertical diffusivity coefficient up to 50 m² s⁻¹ in
 case of unstable stratification. A no-slip lateral boundary
 condition is used and the bottom friction is quadratic. The
 TVD (Total Variance Dissipation) scheme [*Barnier et al.*,
 2006] is used for the tracer advection. NEMOMED8 con-
 serves energy and enstrophy. The solar radiation can pene-
 trate into the ocean surface layers [*Bozec et al.*, 2008].

2.2. Forcings

2.2.1. Surface Boundary Conditions: Atmospheric Forcing

[8] To prescribe air-sea fluxes to the ocean model, we use
 the results of a high-resolution atmospheric data set named
 ARPERA obtained by performing a dynamical downscaling
 of ECMWF fields. Based on the study of the real case of

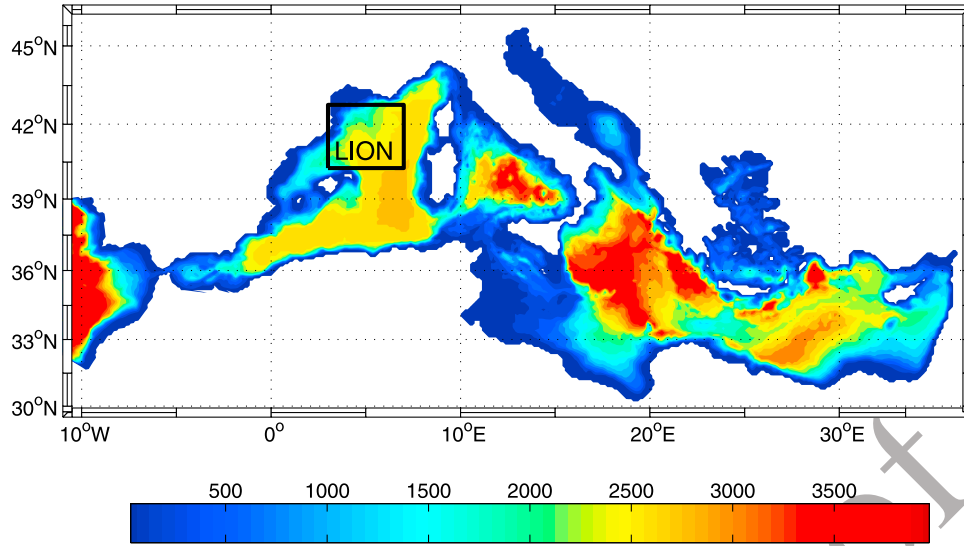


Figure 1. Bathymetry of the modeled domain. The black box corresponds to the LION area, from 3°W to 7°W and from 40.25°N to 42.75°N. Unit is meters.

161 winter 1986–1987, *Herrmann and Somot* [2008] showed that
 162 this data set followed very well the real atmospheric chro-
 163 nology and was relevant to model realistically deep con-
 164 vection in the NWMED. The downscaling method was
 165 described in detail by *Guldborg et al.* [2005]. The principle is
 166 to use a high-resolution atmospheric model, here ARPEGE-
 167 Climate [Déqué and Piedelievre, 1995], in which small
 168 scales can develop freely and large scales are driven by
 169 ECMWF fields. The synoptic chronology then follows that
 170 of ECMWF fields while the high-resolution structures of the
 171 atmospheric flow are created by the model. For the period
 172 1958–2001, fields of ERA40 reanalysis [Gibson et al., 1997]
 173 are used to drive ARPEGE-Climat. Between 2002 and
 174 2006, fields of ECMWF analysis are used, their resolution
 175 (0.5° ~ 55 km) being downgraded down to ERA40 resolution
 176 (1.125° ~ 125 km) in order to insure consistency between the
 177 1958–2001 and 2002–2006 periods.

178 [9] The forcing fields for NEMOMED8 are the momen-
 179 tum, freshwater and heat fluxes. A relaxation term toward
 180 ERA40 sea surface temperature (SST) is applied for the heat
 181 flux. This term actually plays the role of a first-order cou-
 182 pling between the SST computed by the ocean model and
 183 the atmospheric heat flux, ensuring the consistency between
 184 those terms. Following *CLIPPER Project Team* [1999], the
 185 relaxation coefficient is $-40 \text{ W m}^{-2} \text{ K}^{-1}$, equivalent to an
 186 8 day restoring time scale.

187 [10] The LION area (see Figure 1) is chosen in order to
 188 cover entirely the region of NWMED deep convection
 189 reported in the literature [Marshall and Schott, 1999].
 190 Figure 2 shows the evolution of the mean September–
 191 November, December–February and September–February
 192 surface heat, water and buoyancy losses over LION (HL , WL
 193 and BL) between winters 1961–1962 and 2005–2006. The
 194 following formula [Mertens and Schott, 1998] is used for BL :

$$BL = g \cdot \left(\frac{\alpha \cdot HL}{\rho_0 \cdot C_p} - \beta \cdot SSS \cdot WL \right) = BL_H + BL_W \quad (1)$$

where $g = 9.81 \text{ m s}^{-2}$ is the gravitational acceleration, $\rho_0 =$
 1020 kg m^{-3} is the density reference, $C_p = 4000 \text{ J kg}^{-1} \text{ K}^{-1}$ is
 the specific heat of water, $\alpha = 2.10^{-4} \text{ K}^{-1}$ and $\beta = 7.6.10^{-4}$ are
 the thermal and saline expansion coefficients and SSS is the
 sea surface salinity. In agreement with what was previously
 observed by *López-Jurado et al.* [2005] using NCEP [Kalnay
et al., 1996] and by *Font et al.* [2007] using the data of
 the Portbou station from the Catalan Meteorological service,
 the ARPERA data set shows that winter 2004–2005 was the
 coldest and second driest winter of the 1961–2006 period,
 hence the one with the strongest buoyancy loss (highest
 values of $HL = 265 \text{ W m}^{-2}$ versus $147 \pm 47 \text{ W m}^{-2}$ in average
 over the 1961–2006 period, $WL = 4.42 \text{ mm d}^{-1}$ versus $2.96 \pm$
 0.79 mm d^{-1} and $BL = 1.42 \cdot 10^{-7} \text{ m}^2 \text{ s}^{-3}$ versus 0.80 ± 0.24
 $\cdot 10^{-7} \text{ m}^2 \text{ s}^{-3}$). This was due to the occurrence of several
 intense atmospheric events associated with strong winds and
 to cold and dry air masses, during which HL and WL exceeded
 500 W m^{-2} and 10 mm d^{-1} , respectively. This is shown in
 Figure 3a where we present the evolution of the daily average
 over LION between December 2004 and April 2005 of HL ,
 WL , BL and the wind velocity computed in ARPERA and of
 the wind velocity given by QuikSCAT LEVEL 3 data set
 [Perry, 2001] (available on [http://podaac.jpl.nasa.gov:2031/](http://podaac.jpl.nasa.gov:2031/DATASET_DOCSqscat_l3.html)
 DATASET_DOCSqscat_l3.html). Events of strong buoy-
 ancy loss are highlighted in gray in Figure 3. As already
 shown by *Herrmann and Somot* [2008] for winter 1986–
 1987, ARPERA follows very well the real atmospheric
 chronology for winter 2004–2005: the modeled wind velocity
 is correlated with the observed wind velocity obtained from
 QuikSCAT with a correlation factor of 0.970 (significant level
 >0.999). The wind intensity is also correctly reproduced:
 the mean value over LION between December 2004 and
 March 2005 is equal to 8.32 m s^{-1} in ARPERA versus 9.12 m
 s^{-1} in QuikSCAT, with a RMSE of 1.67 m s^{-1} .

2.2.2. Lateral Boundary Conditions: River, Black Sea and Atlantic Forcings

[11] No salinity damping is used at the surface and a
 freshwater flux due to rivers runoff is explicitly added to

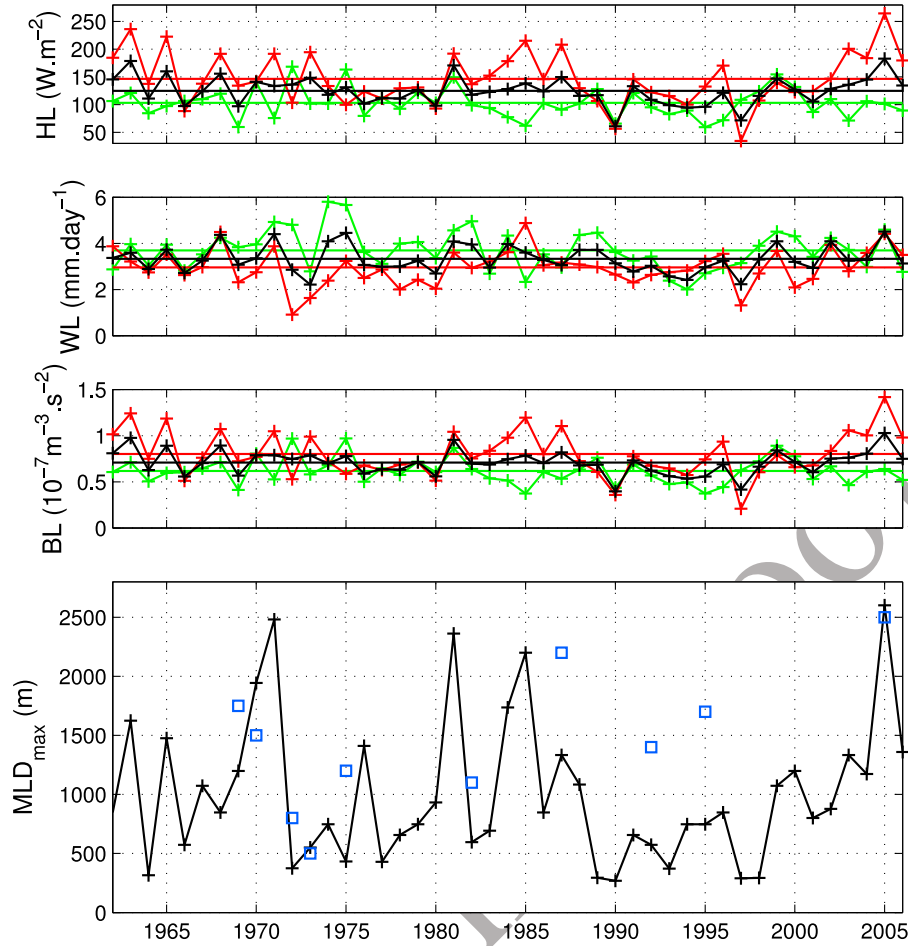


Figure 2. Atmospheric forcing and deep convection: time series of the average autumn (September–November, green), winter (December–February, red), and autumn plus winter (September–February, black) surface heat loss (HL), water loss (WL), and buoyancy loss (BL) over LION in ARPERA and of the winter maximum of the spatial maximum of MLD over LION (MLD_{\max}) between winter 1961–1962 and winter 2005–2006. Here 1965 corresponds to winter 1964–1965. For the atmospheric fluxes the horizontal lines indicate the mean values over 1961–2005. Blue squares correspond to observed MLD values available through several oceanographic cruises and reported by Mertens and Schott [1998], Testor and Gascard [2006], and Schröder et al. [2006].

233 complete the surface water budget. Here we use a monthly
 234 mean climatology (constant over the years) computed from
 235 the RivDis database [Vörösmarty et al., 1996] for the main
 236 33 rivers of the Mediterranean Sea catchment basin.

237 [12] The Black Sea, not included in NEMOMED8, is one
 238 of the major freshwater sources for the Mediterranean Sea.
 239 The exchanges between the Black Sea and the Aegean
 240 subbasin consist of a two-layer flow across the Marmara Sea
 241 and the Dardanelles Strait. We assume that this flow can be
 242 approximated by a freshwater flux diluting the salinity of the
 243 mouth grid point. Thus, the Black Sea is considered as a

river for the Aegean. We use a monthly mean climatology
 for this net flux based on the data collected by Stanev et al.
 [2000].

[13] The exchanges with the Atlantic Ocean are performed
 through a buffer zone from 11°W to 7.5°W . Temperature
 and salinity in this area are relaxed toward the 3-D T-S
 fields of the seasonal Reynaud et al. [1998] climatology by
 means of a Newtonian damping term in the tracer equation
 equal to $-(X_{\text{model}} - X_{\text{climatology}})/\tau$. The restoring term is weak
 close to the Gibraltar Strait ($\tau = 100$ days at 7.5°W) and
 stronger moving away from it ($\tau = 3$ days at 11°W).

Figure 3. (a) Time series during winter 2004–2005 of the average over LION of the daily wind velocity in ARPERA (black) and QuikSCAT (gray) and of the surface heat, water, and buoyancy losses (HL , WL , BL) in ARPERA. For the buoyancy loss, the thin black (gray) line corresponds to the contribution of the water loss (BL_W) (heat loss (BL_H)), and the thick line corresponds to the total BL ($= BL_H + BL_W$). (b) Time series of the maximum MLD over LION, MLD_{\max} , and of the volume of WMDW formed during winter 2004–2005, V_{DW} , for each simulation performed under the atmospheric forcing of 2004–2005 (CLXX and year 2004–2005 of CTRL and NEMT).

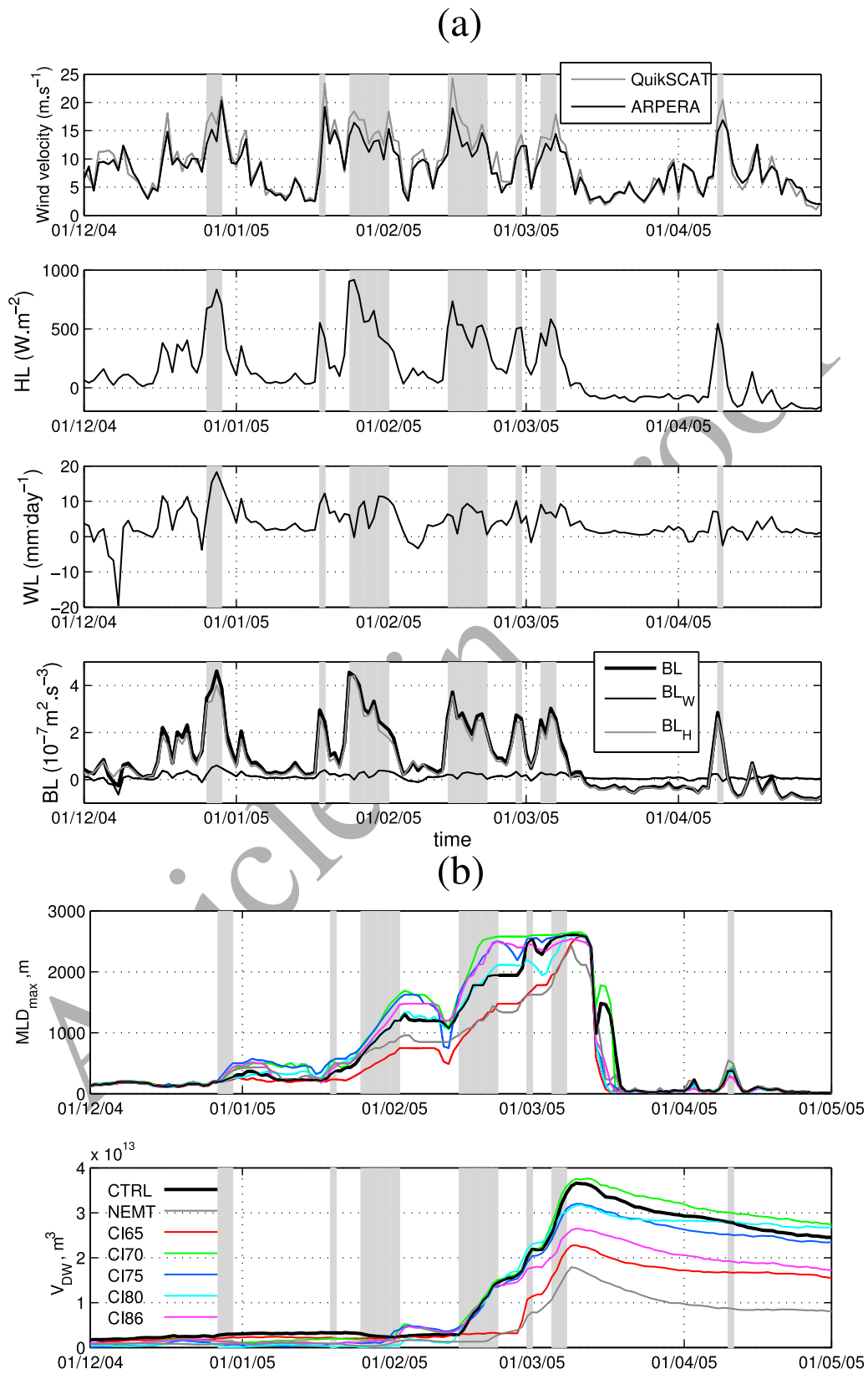


Figure 3

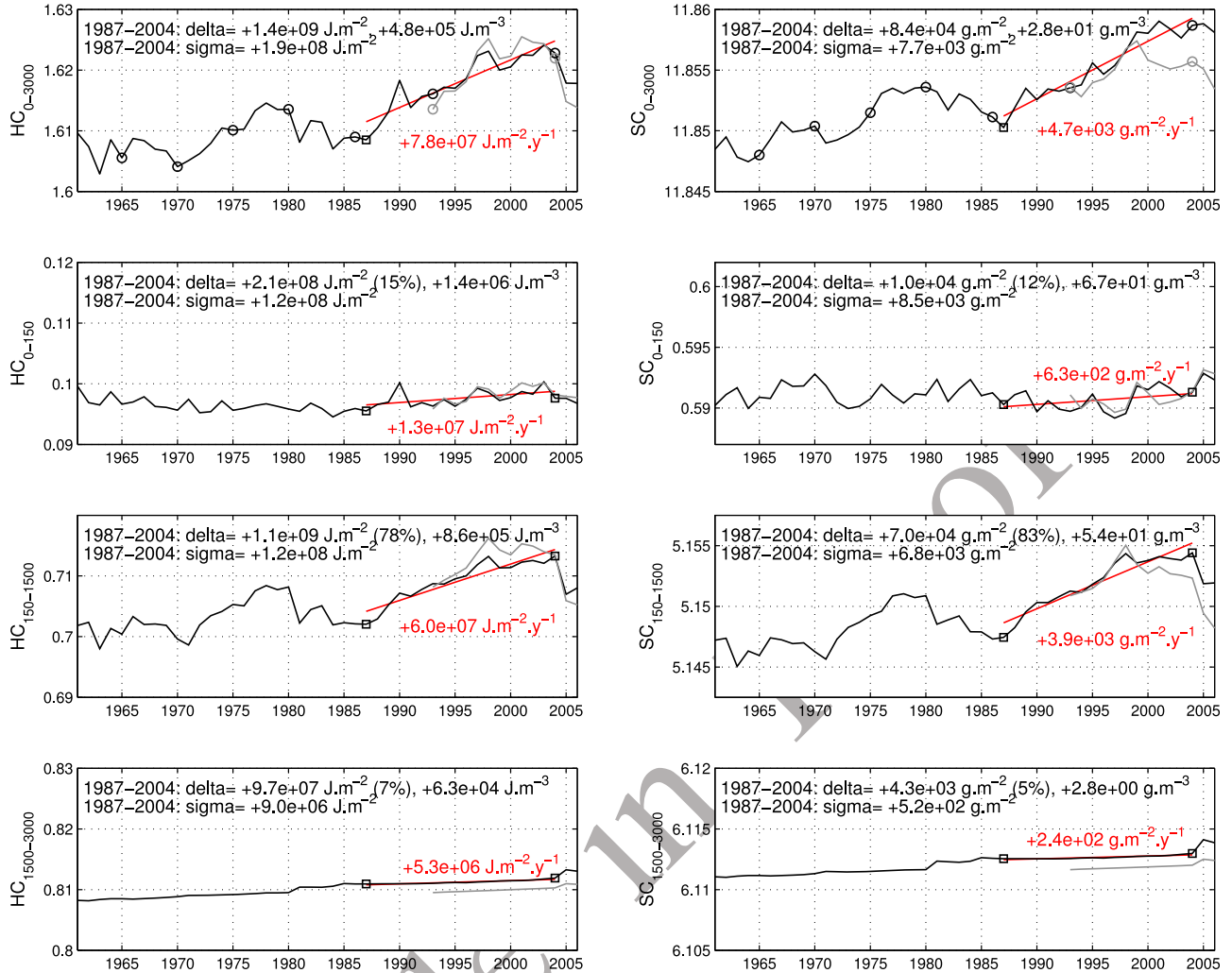


Figure 4. Time series of the mean August (left) heat (HC , 10^{11} J m^{-2}) and (right) salt (SC , 10^7 g m^{-2}) contents of the average water column over LION between 1961 and 2006 in CTRL (black) and between 1993 and 2006 in NEMT (gray) for the whole water column (top line) and the layers 0–150 m (second line), 150–1500 m (third line), and 1500 m to bottom (bottom line). The red line shows the trend between 1987 and 2004 in CTRL, obtained from a linear regression analysis. The value of the trend is indicated in red. Delta indicates the variation of those contents between August 1987 and August 2004 in CTRL, the contribution of each sublayer to the total variation, and the variation of the volumic contents. Sigma is the standard deviation of the time series between 1987 and 2004 in CTRL after the trend has been removed. Circles indicate the years selected to perform the sensitivity simulation CLXX. Squares indicate years 1987 and 2004.

2.3. Simulations

[14] To answer to the scientific questions posed in section 1, we performed several numerical simulations.

2.3.1. Control Simulation CTRL

[15] *Beuvier et al.* [2010] performed an oceanic simulation of the Mediterranean circulation for the 1960–2000 period with NEMOMED8, using the forcings presented above for the surface and lateral boundary conditions (run NM8-ctrl in their paper). The details of this simulation (initial conditions, spin-up) are given in their paper. The initial conditions are given by the MEDATLAS-II climatology [MEDAR/MEDATLAS Group, 2002] for the Mediterranean part of the model, and by the *Reynaud et al.* [1998] climatology for the Atlantic buffer zone. A 15 year

spin-up was then performed before to launch the simulation in August 1960. *Beuvier et al.* [2010] showed that the EMT was realistically reproduced in this simulation: due to an accumulation of dense water in the Aegean during the 1980s and beginning of the 1990s, plus a strong buoyancy loss over the Aegean during winters 1991–1992 and 1992–1993, very dense water ($\rho > 29.2 \text{ kg m}^{-3}$) filled 75% of the Aegean in 1993. This water then cascaded through the Cretan Arc sills into the Ionian and Levantine subbasins and propagated through the rest of the Eastern basin. They also validated the evolution over the period 1960–2000 of the heat and salt contents of the different layers of the Mediterranean Sea, by comparing them to the interannual values given by *Rixen et al.* [2005].

Table 2. Simulations Used in This Study: Name of the Simulation, Atmospheric Forcing Used During the Simulation, and Oceanic Conditions at the Beginning of the Simulation

Name	Atmospheric Forcing: ARPERA	Initial Oceanic Conditions
CTRL	Aug 1960 to Aug 2005	After the initial spin-up: Aug 1960
CI65	Aug 2004 to Aug 2005	Aug 1965 of CTRL
CI70	Aug 2004 to Aug 2005	Aug 1970 of CTRL
CI75	Aug 2004 to Aug 2005	Aug 1975 of CTRL
CI80	Aug 2004 to Aug 2005	Aug 1980 of CTRL
CI86	Aug 2004 to Aug 2005	Aug 1986 of CTRL
AF65	Aug 1965 to Aug 1966	Aug 2004 of CTRL
AF70	Aug 1970 to Aug 1971	Aug 2004 of CTRL
AF75	Aug 1975 to Aug 1976	Aug 2004 of CTRL
AF80	Aug 1980 to Aug 1981	Aug 2004 of CTRL
AF86	Aug 1986 to Aug 1987	Aug 2004 of CTRL
NEMT	Aug 1993 to Aug 2005	Aug 1980 of CTRL

[16] For this study, we extended this simulation until 2006, still using the same forcings (ARPERA for the atmospheric fluxes, *Vörösmarty et al.* [1996] for the rivers, *Stanev et al.* [2000] for the Black Sea and *Reynaud et al.* [1998] for the Atlantic Ocean). In the following, this simulation is named CTRL.

2.3.2. Sensitivity Simulations

2.3.2.1. Impact of the Oceanic Conditions on the Deep Convection Event: Simulations CIXX

[17] To investigate the influence of oceanic conditions on the convection event, we performed a first group of sensitivity simulations varying the oceanic conditions before the beginning of the convection event, i.e., in August 2004. For that, we selected contrasted initial oceanic conditions from the CTRL simulation: we considered the mean August heat and salt contents over the whole water column in LION (Figure 4) and selected five contrasted oceanic conditions before the beginning of the EMT, i.e., before 1987: 1965, 1970, 1975, 1980 and 1986. The heat and salt contents over LION, HC (unit: $J m^{-2}$) and SC (unit: $g m^{-2}$), are computed using the following formula:

$$HC = \frac{1}{A_{LION}} \times \iint_{LION} c_p \rho(x, y, z) T(x, y, z) dx dy dz$$

$$SC = \frac{1}{A_{LION}} \times \iint_{LION} \rho(x, y, z) S(x, y, z) dx dy dz \quad (2)$$

where $A_{LION} = 9.40 \cdot 10^{10} m^2$ is the surface of the LION area. The division by A_{LION} is done in order to obtain an average surfacic value for a column of $1 m^2$ of the LION area, so that we will be able to compare it with the surface and lateral fluxes in the following. Five simulations were then launched in August 2004 using those oceanic conditions as initial conditions, and the same atmospheric conditions as CTRL, i.e., ARPERA from August 2004. Those simulations are named CI65, CI70, CI75, CI80 and CI86 in the following.

2.3.2.2. Impact of the Atmospheric Conditions on the Deep Convection Event: Simulations AFXX

[18] We performed a second group of sensitivity simulations in order to investigate the influence of atmospheric forcing during the convection event: we ran five simulations from August to May taking the same initial oceanic conditions, those of August 2004 of CTRL, but varying the atmospheric forcing. For that we took the atmospheric

forcing of August 1965 to May 1966, August 1970 to May 1971, August 1975 to May 1976, August 1980 to May 1981 and August 1986 to May 1987 from ARPERA. Those simulations are named AF65, AF70, AF75, AF80 and AF86 in the following.

2.3.2.3. Impact of the EMT on the 2005 Convection Event: Simulation NEMT

[19] One of our main objectives is to determine the impact of the EMT on the NW MED convection event of 2004–2005. For that, we performed an additional simulation beginning in August 1993, i.e., just after the EMT, but with the oceanic conditions of August 1980, which are close to August 1993 from the point of view of the heat and salt contents (see Figure 4). This simulation is called NEMT. It cannot contain the EMT signal that occurred between 1987 and 1993, but it is influenced by the same long-term (1993–2004) external forcings as CTRL (surface, hydrologic and lateral boundary conditions). The differences between NEMT and CTRL can therefore be mainly attributed to the impact of the EMT.

[20] The characteristics of the simulations performed for this study are summarized in the first three columns of Table 2: name of the simulation, atmospheric forcing and initial oceanic conditions.

3. Results

3.1. Characteristics of the NW MED Water Column Between 1960 and 2004: Long-Term Evolution and Influence of the EMT

[21] In this section we examine the factors responsible for the evolution until autumn 2004 of the oceanic conditions in the NW MED in terms of heat and salt contents and structure of the water column.

3.1.1. Evolution of the Heat and Salt Contents

[22] *Schroeder et al.* [2010] observed that the salt and heat contents of the water column in the NW MED were anomalously high in 2004. This is reproduced in the CTRL simulation: between August 1987 and August 1998, the heat and salt contents in LION increase regularly, then remain relatively stable until August 2004 (Figure 4). As a result, between 2000 and 2004, these contents are the highest of the whole 1960–2005 period. Between 1987 and 2004, the variation of heat and salt contents are equal to $1.4 \cdot 10^9 J m^{-2}$ and $8.4 \cdot 10^4 g m^{-2}$, respectively. Performing a linear regression analysis, we compute trends of those contents between 1987 and 2004 of $+7.8 \cdot 10^7 J m^{-2} yr^{-1}$ and $+4.7 \cdot 10^3 g m^{-2} yr^{-1}$, respectively. The standard deviations of the detrended signals are equal to $1.9 \cdot 10^8 J m^{-2}$ and $7.7 \cdot 10^3 g m^{-2}$, respectively: those values are 1 order smaller than the values of the variation between 1987 and 2004. The increase observed during this period is therefore statistically significant and not simply due to the interannual variability.

[23] *Schroeder et al.* [2008] suggested that these anomalously high contents could be partly due to an anomalously high arrival of heat and salt from the Eastern basin. However, the regularity of this increase in the model suggests that it is not the case. Moreover, the evolution of the heat and salt contents is very similar in NEMT (Figure 4), which, by construction, does not contain any signal due to the EMT contrary to CTRL. This shows that this increase of heat and salt contents, whatever its origin, was not related to the

381 EMT. Note that on 1 December 2004, the heat contents are
382 quasi equal in NEMT and CTRL, but that the salt content is
383 slightly higher in CTRL. This suggests that the EMT
384 accentuated the salt content increase, perhaps by increasing
385 the salt content of the intermediate and deep water masses
386 originating from the Eastern basin and circulating in the
387 NW MED. Nevertheless this effect is small compared to the
388 long-term increase occurring during the 1990s.

389 [24] *Schroeder et al.* [2010] observed that the high heat
390 and salt contents in 2004 were related to an intermediate
391 layer warmer and saltier than the average: they showed that
392 the difference compared to the climatology was the stron-
393 gest in the 500–1000 m layer. The evolution of the heat and
394 salt contents in each main layer of the average water column
395 over LION in CTRL and NEMT is indicated in Figure 4:
396 surface layer of Atlantic Water (0–150 m), intermediate
397 layer of Levantine Intermediate Water (LIW, 150–1450 m)
398 and deep layer of WMDW (1450 m to bottom). The values
399 obtained for the variation of heat and salt contents between
400 1987 and 2004 in each layer are indicated for CTRL in
401 Figure 4, as well as the values of the contribution of each
402 layer to the total variation, the trend between 1987 and
403 2004, and the standard deviation of the detrended signal
404 between 1987 and 2004. In the intermediate and deep layers,
405 the 1987–2004 variation is 1 order of magnitude larger than
406 the standard deviation of the detrended signal. The increase
407 in these layers is therefore significant and not due to the
408 interannual variability. On the contrary, in the surface layer,
409 the variation between 1987 and 2004 is of the same order
410 than the standard deviation of the detrended signal: the
411 difference between 1987 and 2004 cannot be clearly
412 attributed to a positive trend, but is rather due to the inter-
413 annual variability. This can be explained by the fact that
414 contrary to the deep and intermediate layers, the surface
415 layer is directly submitted to the strong seasonal variability
416 of the atmospheric forcing. Finally during the 1990s, the
417 heat and salt contents significantly increase only in the deep
418 and intermediate layers. The warming and salting of the
419 whole water column is mainly due to the warming and
420 salting of the intermediate layer that represent 78% and
421 83%, respectively, of the total increase.

422 [25] The evolution between 1961 and 2006 in CTRL of
423 the yearly maximum of the spatial maximum of the daily
424 mixed layer depth (MLD) over LION, MLD_{max} , is pre-
425 sented in Figure 2 (black line for CTRL). Comparing the
426 evolution of MLD_{max} with the evolution of the total heat and
427 salt contents shows that those contents increase during the
428 periods of weak convection (1971–1979, 1988–1998) and
429 decrease or remain approximately constant during the peri-
430 ods of stronger convection (1961–1970, 1981–1987, 1999–
431 2006). Indeed, when deep convection occurs, the water
432 column is mixed, producing WMDW. When convection
433 ceases after the winter, the salt and heat originally contained
434 in the warm and salty intermediate layer are exported with
435 the WMDW in the deep layer then out of the convection
436 area [*Herrmann et al.*, 2008]. This results in a transfer of
437 heat and salt from the intermediate layer into the deep layer.
438 This abrupt removal (input) of heat and salt from the
439 intermediate layer (into the deep layer) was observed by
440 *Schroeder et al.* [2010] after the convection event of winter
441 2004–2005. It is reproduced in CTRL, for example after the
442 strong convection events of winters 1980–1981 and 2004–

2005, that both occurred after several winters without deep
convection (Figures 4 and 2). Salt and heat are then pro-
gressively reintroduced in the intermediate layer when the
salty and warm LIW originating from the Eastern basin
[*Millot*, 1999] spreads into the NW MED. If convection does
not occur during a few years, the heat and salt contents of
the intermediate layer will therefore increase until warm and
salty LIW has completely refilled this layer. As will be
shown in section 3.3.1, the intensity of deep convection
depends on the winter buoyancy loss: deep convection
occurs when the winter buoyancy loss is sufficiently strong,
enabling the initially stratified water column to be mixed to
great depth. Between 1988 and 2001, the winter buoyancy
loss was generally lower than the average, explaining that
convection was weak during this period (Figure 2). Our
results therefore suggest that the exceptionally high heat and
salt contents in 2004 were not due to an anomalously high
arrival of heat and salt induced by the EMT, but to the
absence of strong convection during the 1990s. This absence
would have resulted from the weakness of the winter
atmospheric buoyancy loss during this period and enabled
the heat and salt to accumulate in the intermediate layer.

[26] Observed values of MLD available thanks to several
oceanographic campaigns reported by *Mertens and Schott*
[1998], *Testor and Gascard* [2006] and *Schröder et al.*
[2006] are also indicated in Figure 2 (blue squares). Com-
paring the data and the model results suggests that the
absolute value of the modeled MLD is generally under-
estimated. Data are, however, too scarce to validate the
representation of the interannual variability of the MLD,
which is suggested here to play an important role in the long-
term evolution of heat and salt content in the Gulf of Lion.
Nevertheless, this comparison put our conclusions into per-
spectives, reminding that they are obtained thanks to a given
model forced by a given atmospheric data set. We analyze
and interpret the results of this model, which is not the reality
but a tentative to represent it as well as possible using the
state of the art of the models used to simulate the long-term
Mediterranean oceanic circulation. It would be necessary to
perform a group of other simulations using other ocean
models and other atmospheric forcing in order to enforce the
robustness of our conclusions or to propose alternative
explanations. Note, however, that other studies [*Sannino*
et al., 2009] also suggest that due to weak winter surface
buoyancy flux, the 1990s was a period of weak convection.

3.1.2. Impact of the EMT on the Structure of the Water Column

[27] Analyzing hydrographic data, *Gasparini et al.* [2005]
showed that in the Sicily channel and in the Tyrrhenian
subbasin, the EMT resulted in a deepening between 1992
and 2003 of the heat and salt originating from the Eastern
Basin. As a result the saltier and warmer waters progres-
sively extended their influence in depth until 1500 m (see
Figure 14 of *Gasparini et al.* [2005]). Deep water of eastern
origin then flows into the NW MED [*Millot*, 1999], we can
therefore expect from those observations in the Tyrrhenian
that the EMT induced the deepening of the salty and warm
intermediate layer in the NW MED. Indeed, the heat and salt
increase extended deeper in CTRL (until 1500 m; Figure 5),
in agreement with the observations, than in NEMT where it
mainly occurred in the “classical” intermediate layer (200–
1000 m). Our modeling study therefore shows an effect of

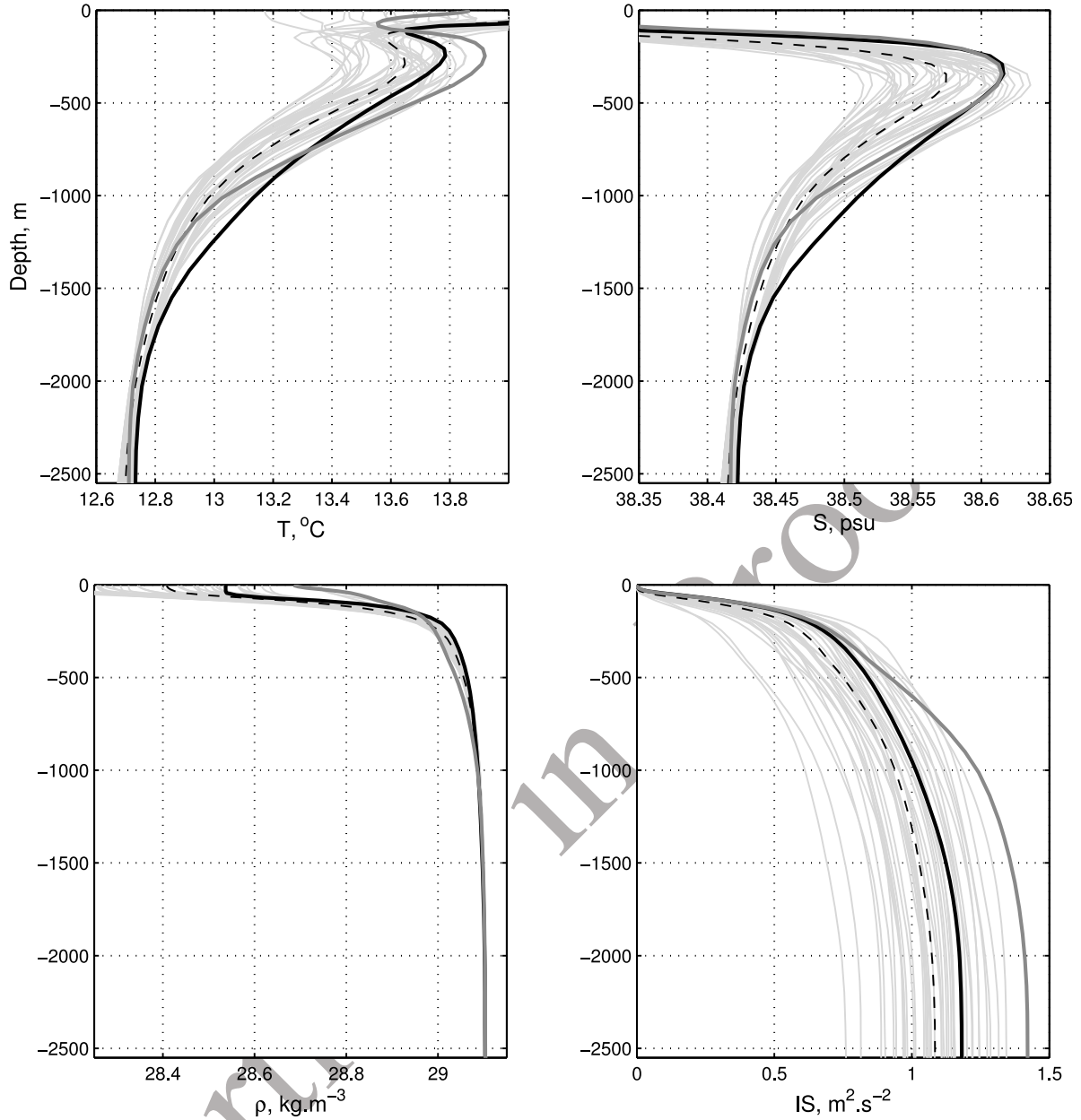


Figure 5. Average temperature, salinity, density, and stratification profiles in December over LION. Light gray lines are 1961–2000 for CTRL. Dashed line is average profile over 1961–2000. Black line is 2004 for CTRL. Dark gray line is 2004 for NEMT.

505 the EMT on the structure of the NWMED water column in
 506 agreement with the observations made by *Gasparini et al.*
 507 [2005] and *Schroeder et al.* [2010]: the EMT induced a
 508 deepening of the heat and salt maximum in the NWMED.
 509 [28] *Gasparini et al.* [2005] showed that this deepening
 510 was associated with an increase of the density of the warm
 511 and salty eastern waters flowing in the intermediate and
 512 deep layers of the Western basin. This increase of the
 513 density in the intermediate layer is reproduced by the model,
 514 as can be seen when comparing the CTRL and NEMT
 515 density profiles (Figure 5). The vertical density gradient
 516 in these layers consequently decreased. To investigate
 517 the effect of this modification of the density profile on the
 518 stratification of the NWMED water column, we compute the

total buoyancy flux required to mix an initially stratified
 water column down to the depth z , $IS(z)$, using the formula
 used by *Herrmann et al.* [2008]:

$$IS(z) = \int_0^z N^2(h) \cdot h \cdot dh = \int_0^z \frac{-g}{\rho} \frac{\partial \rho}{\partial h} \cdot h \cdot dh \quad (3)$$

where N (s^{-1}) is the initial Brunt-Väisälä frequency. IS
 represents an index of the stratification of the water column.
 The stratification profiles on December 2004 over LION are
 shown in Figure 5 for CTRL and NEMT. The stratification
 in NEMT is among the strongest of the whole 1961–2004
 period, whereas the stratification in CTRL is only slightly
 above the average. This shows that the EMT induced a

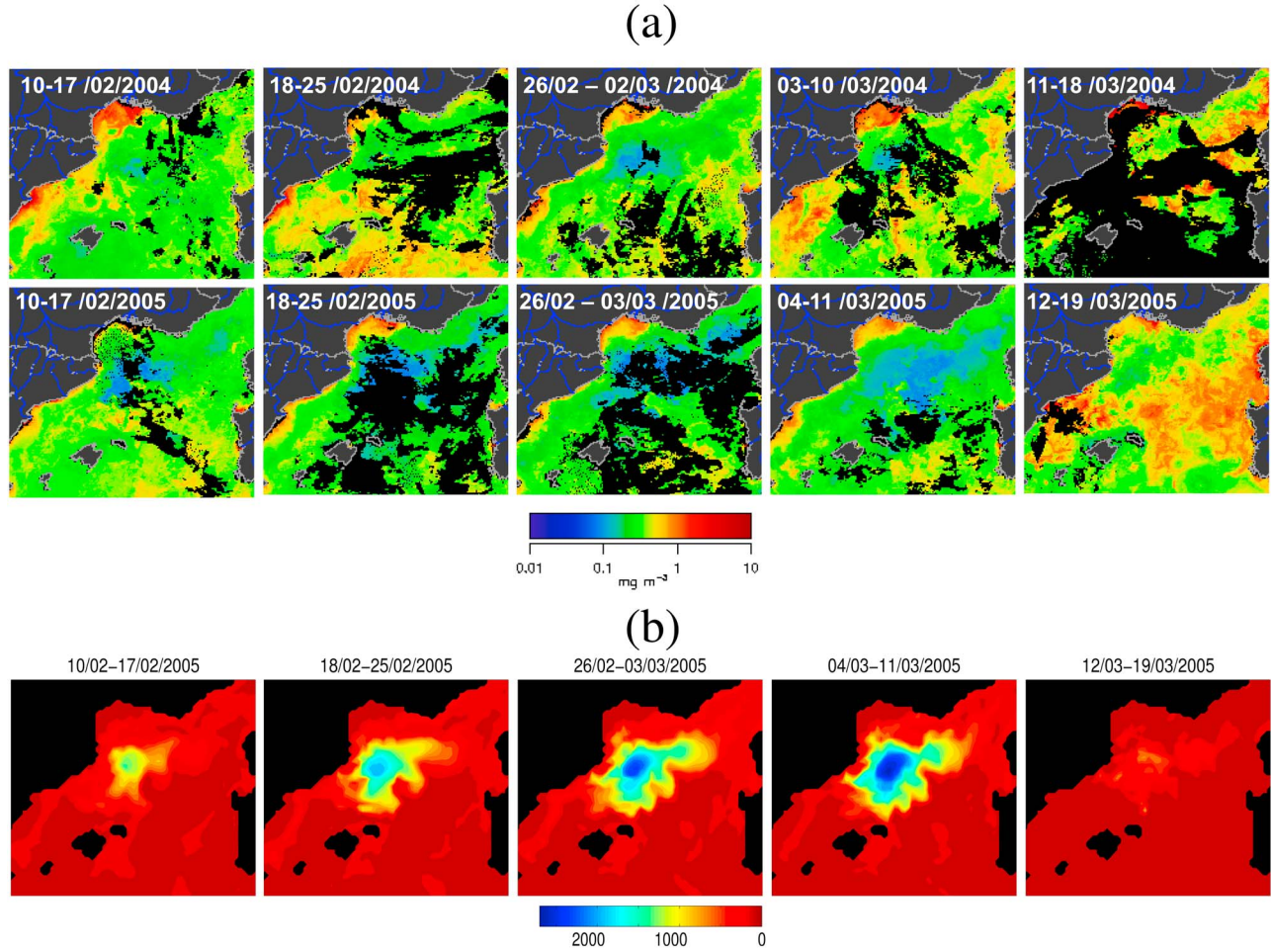


Figure 6. (a) Weekly averaged surface chlorophyll concentration observed by MODIS in the NWMED during the winter convection period (mid-February/mid-March) in (top) 2004 and (bottom) 2005 (unit is mg m^{-3}). (b) Maps of the MLD averaged over the same periods in CTRL (unit is meters).

weakening of the NWMED stratification compared with what would have been the case without the EMT. This is due to the fact that $IS(z)$ being proportional to $\int z \times \frac{\partial \rho}{\partial z}$, a decrease of the vertical density gradient in the intermediate and deep layer results in a decrease of IS .

3.2. Modeling of the 2005 NWMED Convection Event: Validation of the CTRL Simulation

[29] All the information concerning the 2004–2005 convection event available to us was gathered in order to validate the modeling of this event in CTRL. First, in situ observations available in the literature cited in section 1 provide information about the hydrologic characteristics and the structure of the water column in the WMDW and about the characteristics of the WMDW. Second, satellite ocean color data provide information about the temporal and spatial evolution of the convection process.

3.2.1. Temporal and Spatial Characteristics of the 2005 Convection Event

[30] The deepest value of MLD_{\max} between 1961 and 2006 in CTRL is obtained for 2004–2005 (2601 m), one of the four winters of the whole period during which the convection reaches the bottom ($MLD > 2000$ m) in this

simulation (Figure 2). Convection during winter 2004–2005 is therefore exceptionally strong in CTRL, in agreement with the reported observations.

[31] MODIS Ocean color data available on <http://marine.jrc.ec.europa.eu> provide an estimate of the extension of the convection area. In this area, strong vertical displacements indeed prevent the phytoplankton from remaining at the surface. The convection area therefore corresponds to the region of low chlorophyll concentration. Figure 6a shows the maps of the 8 day average chlorophyll obtained from MODIS between 10 February and 18 March 2004 and 2005. Comparing the 2004 and 2005 maps shows that the particularly large extension of the convection area in 2005 is well captured by those images.

[32] The extension of the low chlorophyll area is the largest between 18 February and 11 March 2005, indicating that this period was the period of maximum convection. Convection does not seem to occur after 12 March. This is in agreement with *Smith et al.* [2008] who reported that the water column was strongly mixed in the Catalan sea between 7 and 12 March.

[33] WMDW is identified in our simulations as the water of density larger than 29.1 kg m^{-3} , following previous

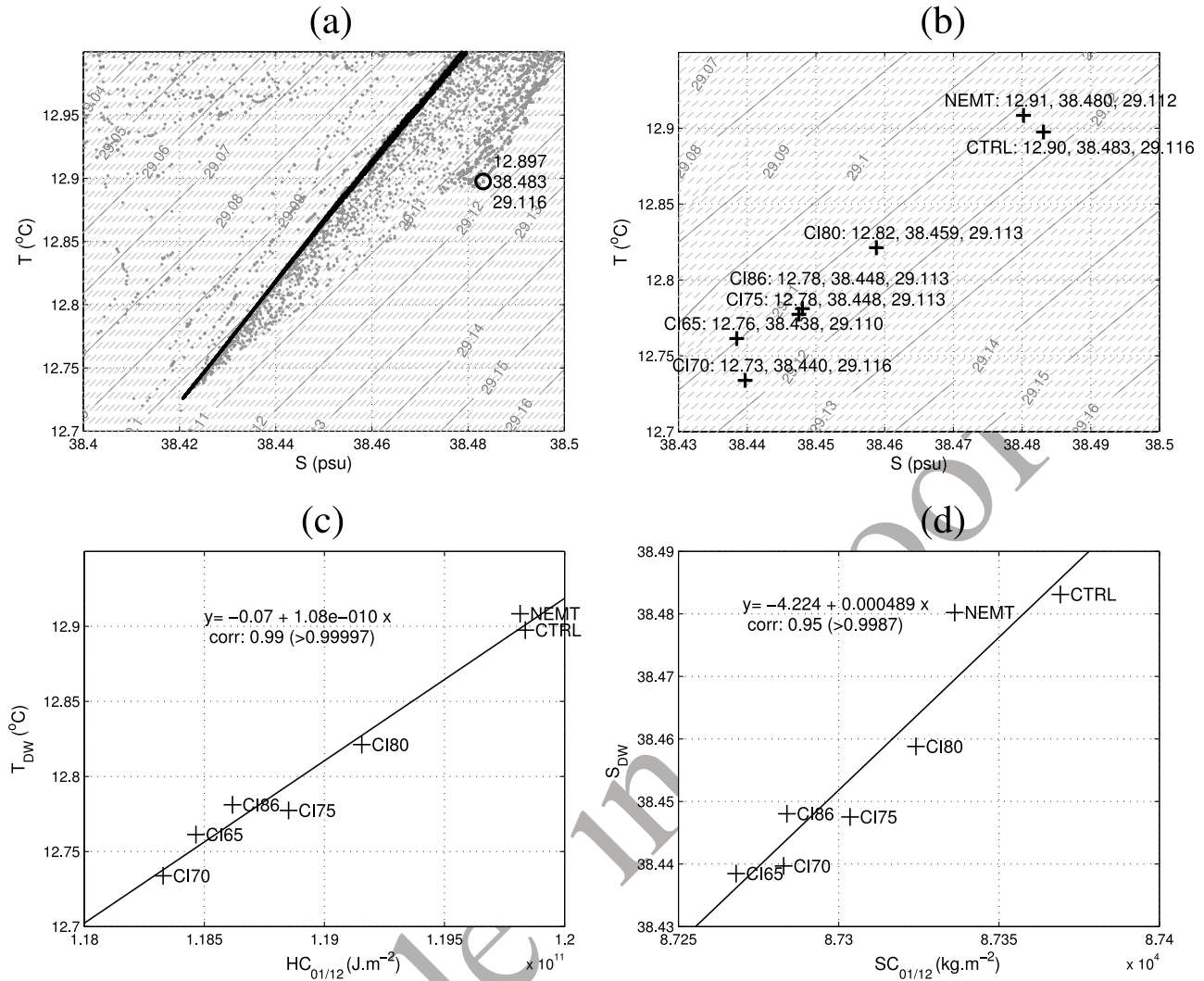


Figure 7. WMDW characteristics in simulations performed under the atmospheric forcing of 2004–2005. (a) Temperature-salinity diagram of the water present in LION over the whole column before the convection (1 December 2004, black points) and at the date of maximum convection (10 March 2005, gray points) in CTRL: each point corresponds to a point of the model grid. The characteristics of the densest water present in LION on 10 March 2005 are indicated (black circle). (b) Characteristics (T ($^{\circ}C$), S, ρ ($kg \cdot m^{-3}$)) of the densest water present in LION at the date of maximum convection (10 March 2005) for each simulation. (c) Relation between the preconvective heat content over LION, $HC_{01/12}$, and the WMDW temperature T_{DW} . (d) Relation between the preconvective salt content over LION, $SC_{01/12}$, and the WMDW salinity S_{DW} .

574 modeling and observation studies (see, for example, 575 Marshall and Schott [1999] or Herrmann et al. [2008]). 576 Following Herrmann et al. [2008], the volume of newly 577 formed WMDW V_{DW} is computed each day as the differ- 578 ence between the volume of WMDW present in the 579 NWED on this day and the minimum of this volume 580 before the convection event, i.e., in autumn 2004 (equal to 581 $13.0 \cdot 10^{13} m^3$): V_{DW} represents an anomaly. The WMDW 582 formation rate τ_{DW} is then computed following Castellari 583 et al. [2000] by dividing V_{DW} by the numbers of seconds 584 in 1 year. Times series between 1 December 2004 and 30 585 April 2005 of the modeled maximum MLD over LION 586 MLD_{max} and of V_{DW} are shown in Figure 3b (black line for 587 CTRL). The evolution of the convection event follows the 588 atmospheric chronology: each atmospheric event of strong

buoyancy loss induces an abrupt increase of MLD_{max} and 589 V_{DW} . The mixed layer reaches 1500 m on 17 February, and 590 the bottom is reached between 27 February and 13 March 591 ($MLD_{max} > 2000 m$), with a small decrease between 1 March 592 and 3 March induced by a decrease of buoyancy loss. This is 593 in agreement with the satellite and in situ observations. The 594 maximum of V_{DW} is reached on 10 March after the last 595 atmospheric event. It is equal to $3.66 \cdot 10^{13} m^3$, corresponding 596 to a formation rate τ_{DW} of 1.16 Sv. This value is consistent 597 with Schroeder et al. [2008], who estimated from in situ 598 observations that the cumulated formation rate for winters 599 2004–2005 and 2005–2006 was approximately equal to 600 2.4 Sv. Then, as soon as the atmospheric BL becomes neg- 601 ative, MLD_{max} abruptly decreases to zero: restratification of 602 the water column begins, and V_{DW} starts to decrease. The 603

t3.1 **Table 3.** Preconvection and Convection Characteristics for Each Simulation^a

t3.2	Name ^b	HC on 1 December (10^{11} J m^{-2})	SC on 1 December (10^4 kg m^{-2})	IS on 1 December ($\text{m}^2 \text{ s}^{-2}$)	T_{DW} ($^{\circ}\text{C}$)	S_{DW}	ρ_{DW} (kg m^{-3})	τ_{DW} (Sv)	MLD_{\max} (m)	MLD_{mean} (m)
t3.3	CTRL 2004–2005	1.198	8.737	1.02	12.90	38.483	29.116	1.16	2601	943
t3.4	CTRL 1965–1966	1.184	8.727	1.11	no WMDW			0.07	372	94
t3.5	CTRL 1970–1971	1.185	8.729	1.02	12.81	38.451	29.110	0.42	2398	472
t3.6	CTRL 1975–1976	1.186	8.731	0.90	no WMDW			0.14	1416	264
t3.7	CTRL 1980–1981	1.188	8.733	0.84	12.90	38.479	29.113	0.85	2382	510
t3.8	CTRL 1986–1987	1.188	8.728	1.21	no WMDW			0.06	1333	223
t3.9	CI65	1.185	8.727	1.15	12.76	38.438	29.110	0.72	2584	729
t3.10	CI70	1.183	8.728	0.98	12.73	38.440	29.116	1.19	2645	923
t3.11	CI75	1.189	8.730	1.05	12.78	38.448	29.113	1.02	2604	804
t3.12	CI80	1.192	8.732	1.05	12.82	38.459	29.113	1.01	2593	749
t3.13	CI86	1.186	8.728	1.10	12.78	38.448	29.113	0.84	2543	765
t3.14	AF65	1.198	8.737	1.01	no WMDW			0.06	433	118
t3.15	AF70	1.200	8.737	1.06	13.04	38.513	29.110	0.54	1883	564
t3.16	AF75	1.196	8.737	0.86	no WMDW			0.10	1199	282
t3.17	AF80	1.195	8.738	0.77	12.92	38.488	29.115	1.63	2562	768
t3.18	AF86	1.200	8.736	1.15	no WMDW			0.08	1333	291
t3.19	NEMT 2004–2005	1.198	8.734	1.24	12.91	38.480	29.112	0.57	2429	746

t3.20 ^aGiven are average heat and salt contents and stratification index at 1000 m over LION on 1 December (HC, SC, and IS), WMDW characteristics (T_{DW} ,
t3.21 S_{DW} , and ρ_{DW}), WMDW formation rate (τ_{DW}), winter maximum of the maximum MLD over LION (MLD_{\max}), and winter maximum of the average MLD
t3.22 over LION (MLD_{mean}). When $MLD_{\max} < 1500$ m the convection is not considered as deep but intermediate. No WMDW is formed.
t3.23 ^bYear is also given for CTRL and NEMT.

604 chronology of the convection event reproduced by the model
605 is therefore in good agreement with the chronology deduced
606 from the available observations.

607 [34] The modeled area of convection corresponds to the
608 area obtained from the ocean color data, as can be seen when
609 comparing the maps of the 8 day average of the modeled
610 MLD between 10 February and 18 March shown in Figure 6b
611 and the corresponding ocean color maps. At each period, the
612 size and position of the modeled convection area corresponds
613 to the size and position of the observed low chlorophyll
614 concentration area. The extension of the convection area is
615 the largest between 26 February and 11 March, as the
616 extension of the low chlorophyll concentration area.

617 3.2.2. Characteristics of WMDW Formed in 2005

618 [35] Figure 7a shows the temperature–salinity diagram
619 of the water present in LION before the convection event
620 (1 December 2004) and when the convection reaches its
621 maximum (10 March 2005). “Old” WMDW, i.e., WMDW
622 formed before winter 2004–2005, can be identified on
623 1 December as the water present in LION and denser than
624 29.10 kg m^{-3} : in CTRL, characteristics of old WMDW are
625 $\sim 12.72\text{--}12.80^{\circ}\text{C}$ and $\sim 34.42\text{--}38.44$. They belong to the
626 range of the observed characteristics of old WMDW reported
627 in the literature ($12.75\text{--}92^{\circ}\text{C}$, $38.41\text{--}47$; see Table 1).
628 WMDW formed during winter 2004–2005 can be identified
629 as the densest water present on 10 March. Its characteristics
630 ($T_{DW} = 12.90^{\circ}\text{C}$, $S_{DW} = 38.48$ and $\rho_{DW} = 29.116 \text{ kg m}^{-3}$) are
631 in very good agreement with the observed characteristics of
632 WMDW formed in 2005 ($12.87\text{--}90^{\circ}\text{C}$, $38.47\text{--}50$, 29.113--
633 130 kg m^{-3} ; see Table 1). The change of temperature and
634 salinity between old and “new” WMDW is therefore also
635 correctly reproduced ($\sim +0.1\text{--}0.2^{\circ}\text{C}$ and $\sim +0.04\text{--}0.06$).

636 3.3. Analysis of the Sensitivity Simulations: Which 637 Factors Were Responsible for the Characteristics 638 of the 2005 Convection Event?

639 [36] Having shown that the CTRL simulation represents
640 correctly the 2004–2005 convection event, we now analyze
641 the sensitivity simulations in order to determine the

642 respective contributions of the oceanic and atmospheric
643 conditions to the characteristics of this event.

644 3.3.1. Why Was the 2004–2005 Convection Event 645 Exceptionally Strong?

646 [37] In this section we investigate the factors responsible
647 for the exceptional intensity of the 2005 convection event in
648 terms of mixed layer depth and volume of newly formed
649 WMDW: we examine the influence of the stratification of
650 the water column at the beginning of the convection, of the
651 EMT and of the atmospheric conditions during 2004.

652 3.3.1.1. Impact of the Oceanic Conditions of 2004–2005 653 and of the EMT on the Convection Intensity

654 [38] To investigate the role played by the oceanic condi-
655 tions in the intensity of the 2004–2005 convection event, we
656 examine the simulations where the atmospheric forcing is
657 the one of year 2004–2005 but where the initial oceanic
658 conditions vary: CIXX and year 2004–2005 of CTRL and
659 NEMT. For those simulations, the evolution of the maxi-
660 mum MLD over LION, MLD_{\max} , and of the volume of
661 newly formed WMDW, V_{DW} , is presented in Figure 3b. The
662 chronology of the convection event is the same for all those
663 simulations: each event of strong atmospheric buoyancy loss
664 (highlighted in gray in Figure 3) induces an abrupt deep-
665 ening of the mixed layer and an increase of V_{DW} , which then
666 remain relatively stable. The maximum of the convection
667 intensity, corresponding to the maximum of V_{DW} , is reached
668 for all the simulations on 10 March, just after the last event
669 of strong buoyancy loss occurring in March. At this time,
670 the convection reaches the bottom in all the simulations:
671 MLD_{\max} varies between 2430 m for NEMT and 2645 m for
672 CTRL (Table 3). The MLD then abruptly decreases when
673 the buoyancy loss becomes positive, after 13 March, and
674 V_{DW} begins to decrease.

675 [39] First, this shows that the chronology of the convec-
676 tion in terms of deepening/shallowing of the mixed layer
677 and increase/decrease of V_{DW} is driven by the succession of
678 atmospheric events. For year 2004–2005, this resulted in a
679 strong bottom convection. Second, although bottom con-
680 vection occurs in all those simulations, the volume of newly

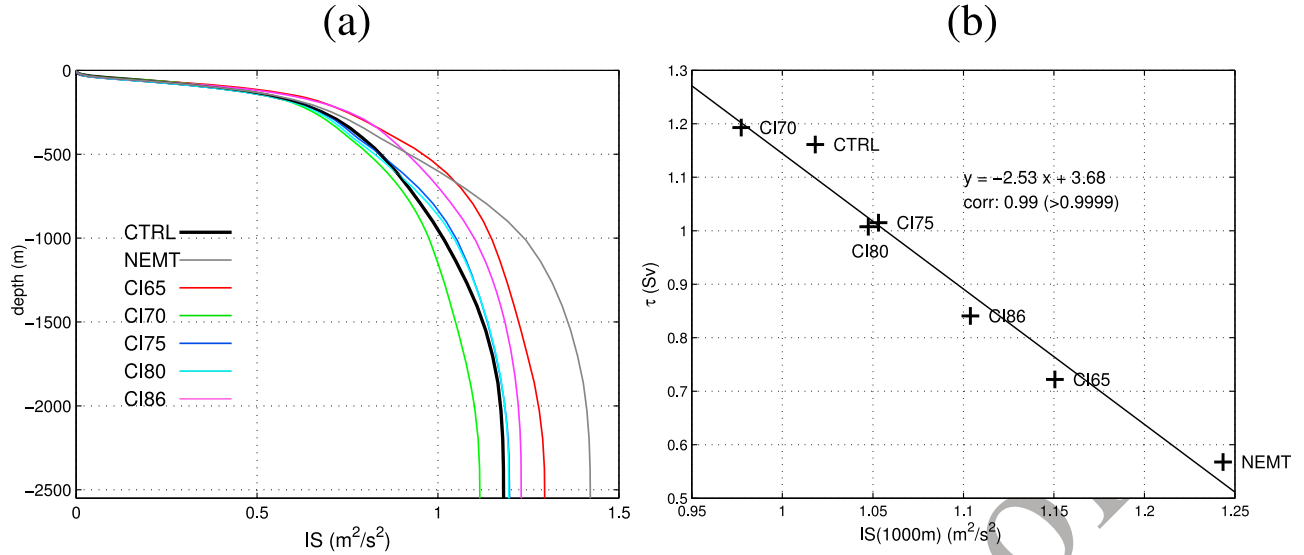


Figure 8. (a) For simulations performed under the 2004–2005 atmospheric forcing, average profile over LION of the stratification index on 1 December, $IS(z)$. (b) Relation between the average stratification index over LION at 1000 m on 1 December 2004, $IS(1000m)$, and the WMDW formation rate, τ_{DW} .

formed WMDW varies by a factor of 2 between the most and the less productive simulations ($\tau_{DW} \sim 0.7$ Sv in CI65 and ~ 1.2 Sv in CI70; Figure 3b and Table 2). This variability of τ_{DW} is actually related to the variability of the stratification of the water column at the beginning of the convection: the more stratified the column is, the more difficult it is to mix it. To show that, we examine the profiles of $IS(z)$ before the convection event on 1 December for year 2004 of NEMT, CTRL and CLXX (Figure 8a). The most stratified water column is obtained in NEMT, and CTRL is among the simulations with the less stratified water column. The largest winter maximum of the average MLD over LION in 2005 is obtained for CTRL; $MLD_{mean} = 943$ m, slightly less than 1000 m (Table 3). We therefore compute for each simulation the stratification index of the water column at 1000 m before the convection event on 1 December 2004 (Table 2). Performing a regression analysis between the WMDW formation rate τ_{DW} and $IS(1000\text{ m}, 1\text{ December } 2004)$, we obtain a strong linear relationship with a correlation factor of 0.99 ($SL > 0.9999$) (Figure 8b). For given atmospheric conditions, here those of winter 2004–2005, the variability of the intensity of deep convection in terms of volume of newly formed WMDW is therefore directly related to the variability of the stratification at the beginning of the convection, which facilitates or hinders the mixing of the water column.

[40] Comparing the IS profiles in December 2004 in NEMT and CTRL, we showed in section 3.1 that the EMT induced a weakening of the stratification in the NWMD. As a result, the intensity of deep convection in terms of WMDW formed is twice stronger in CTRL than in NEMT.

3.3.1.2. Impact of the Atmospheric Conditions of 2004–2005 on the Convection Intensity

[41] Figure 5 shows the profiles of $IS(z)$ before the convection event on 1 December for all the years of the CTRL simulation and for year 2004 of NEMT. The water column on 1 December 2004 in NEMT is the most stratified of all the

years; however, the convection reaches the bottom. This suggests that the atmospheric buoyancy loss in 2004–2005 played the most determining role in the intensity of the convection event: it was so strong that convection could have reached the bottom even for the most stratified conditions.

[42] To confirm the influence of the atmospheric conditions on the intensity of the 2004–2005 convection event, we examine the simulations where the initial oceanic conditions are those of August 2004 but where the atmospheric forcing varies: AFXX and year 2004–2005 of CTRL. For those simulations, the evolution of the atmospheric buoyancy loss, of MLD_{max} and of V_{DW} is presented in Figure 9. The variability of the convection depth and newly formed WMDW volume induced by the atmospheric forcing is much larger than the variability induced by the oceanic conditions: there are simulations with no convection ($AF65$, $MLD_{max} = 433$ m) or intermediate convection ($1000\text{ m} < MLD_{max} < 1500\text{ m}$, AF70, AF86) and practically no WMDW formed ($\tau_{DW} < 0.1$ Sv), and simulations with τ_{DW} varying between 0.5 Sv and 1.6 Sv with deeper convection (AF75, $MLD_{max} = 1883$ m) or even bottom convection ($MLD_{max} > 2000$ m, AF80, CTRL). This confirms that the factor predominantly responsible for the intensity of deep convection in 2004–2005 was the atmospheric forcing rather than the oceanic conditions: with different initial oceanic conditions of another autumn bottom convection would have occurred anyway, whereas with different atmospheric conditions there could have been no convection, intermediate convection or bottom convection.

[43] Which aspect of the atmospheric forcing more precisely drives the convection? We saw that the succession of strong buoyancy loss event induces the deepening of the mixed layer during the winter, corresponding to the violent mixing phase of deep convection defined by Marshall and Schott [1999]. We therefore expect the variability of the intensity of deep convection to be related to the variability of the cumulated buoyancy loss over this phase. However,

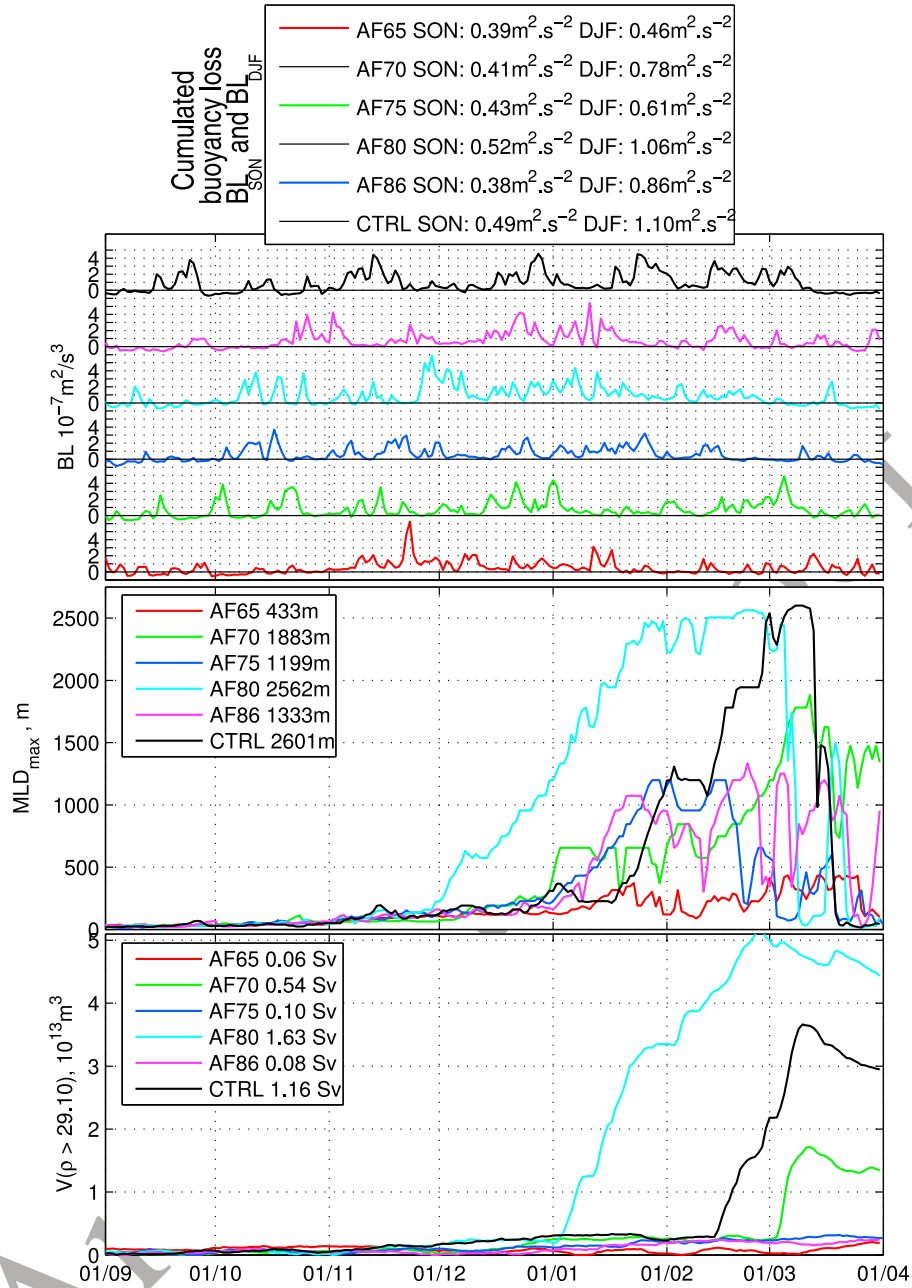


Figure 9. For simulations performed with the initial oceanic conditions of August 2004 of CTRL (AFXX and year 2004–2005 of CTRL), time series between September and March of the average buoyancy loss over LION, BL ; of the maximum MLD over LION, MLD_{\max} ; and of the volume of newly formed WMDW, V_{DW} . For each simulation we indicate the values of (top) the buoyancy loss cumulated over September–November and December–February, of (middle) the maximum of MLD_{\max} , and of (bottom) the WMDW formation rate.

the autumn atmospheric buoyancy loss before this phase, i. e., during the preconditioning phase [Marshall and Schott, 1999], certainly also plays an important role: it participates to the weakening of the stratification of the water column. The times series of the mean atmospheric buoyancy loss over LION during September–November, December–February, and September–February are presented in Figure 2. For simulations performed with the same initial oceanic conditions, the values of the cumulated buoyancy loss

during those periods, BL_{SON} , BL_{DJF} and BL_{SONDJF} , are reported in Figure 9 (top). The results suggest that an atmospheric buoyancy loss stronger than the average is necessary both during the preconditioning and during the violent mixing in order to produce deep convection. In particular, in CTRL and AF80, i.e., the two simulations where convection reaches the bottom, buoyancy losses are significantly stronger than the average over 1960–2006 (BL_{SON} is equal to 0.49 and 0.52 $\text{m}^2 \text{ s}^{-2}$ in CTRL and

AF80, respectively, versus an average value of $0.48 \text{ m}^2 \text{ s}^{-2}$ and BL_{DJF} is equal to 1.10 and $1.06 \text{ m}^2 \text{ s}^{-2}$ versus $0.63 \text{ m}^2 \text{ s}^{-2}$). On the contrary in AF65 and AF75, BL_{SON} (0.39 and $0.43 \text{ m}^2 \text{ s}^{-2}$, respectively) and BL_{DJF} (0.46 and $0.61 \text{ m}^2 \text{ s}^{-2}$, respectively) are both smaller than the average, and the MLD does not exceed 1500 m. However, some situations are not so straightforward: AF86 does not produce deep convection whereas AF70 does, though their values of BL_{DJF} (0.86 and $0.78 \text{ m}^2 \text{ s}^{-2}$, respectively) are both larger than the average and their values of BL_{SON} ($0.38 \text{ m}^2 \text{ s}^{-2}$ and $0.41 \text{ m}^2 \text{ s}^{-2}$, respectively) are both smaller than the average. More generally, examining the time series of the atmospheric buoyancy loss and of the maximum MLD between 1961 and 2006 in CTRL (Figure 2) shows that it is very difficult to find a clear relationship between BL and MLD_{\max} : see for example winters 1969–1970, 1975–1976 and 1986–1987. It would certainly be necessary to consider the influence of other factors like the frequency and duration of the atmospheric events. A much larger amount of simulations would be necessary to build a relevant indicator of atmospheric conditions to which the interannual variability of the intensity of deep convection could be related. This is, however, beyond the scope of this study, that focuses on the 2004–2005 case.

[44] Finally, our sensitivity simulations suggest that the strong atmospheric buoyancy loss observed both during autumn 2004 and winter 2004–2005, i.e., during the preconditioning and the violent mixing, was the major factor at the origin of the intensity of the convection observed this year. The particularly weak stratification of the water column in December 2004 induced by the EMT would have then accentuated the effect of this strong atmospheric conditions and potentially doubled the volume of WMDW formed, but would not have fundamentally modify the convection process.

3.3.2. Why Was the WMDW Formed in 2005

Exceptionally Warm and Salty?

[45] In this section we examine the contributions of the oceanic and atmospheric conditions before and during the convection event of 2004–2005 to the characteristics of the WMDW formed in 2005.

3.3.2.1. Impact of the Oceanic Conditions Before and During the 2004–2005 Convection Event on the WMDW Characteristics

[46] To investigate the influence of the initial oceanic conditions on the characteristics of the WMDW formed in 2004–2005, we examine the simulations where the atmospheric forcing is the one of year 2004–2005 but where the initial oceanic conditions vary: CLXX and year 2004–2005 of CTRL and NEMT (see section 2.3.2). For those simulations, the characteristics of WMDW formed during winter 2004–2005, corresponding to the densest water found in LION at the date of maximum convection (10 March 2005; see section 3.3.1), are indicated in Table 3 and in Figure 7b. WMDW produced in the CLXX simulations corresponds to old WMDW (12.73 – 12.82°C , 38.43 – 38.46 ; see Table 1), whereas WMDW produced in CTRL but also in NEMT corresponds to new WMDW ($\sim 12.9^\circ\text{C}$, ~ 38.48 ; see Table 1). When convection reaches the bottom, which is the case in all the simulations examined here (Figure 3), WMDW is formed by mixing of the whole water column. Therefore, we

can expect the temperature and salinity of newly formed WMDW to depend on the heat and salt contents of this water column just before the convection. To confirm this hypothesis, we perform a linear regression analysis between the WMDW characteristics and the average heat and salt contents over LION on 1 December, $HC_{01/12}$ and $SC_{01/12}$ (Figures 7c and 7d). Values of $HC_{01/12}$ and $SC_{01/12}$ are reported in Table 3. T_{DW} and S_{DW} are linearly related to $HC_{01/12}$ and $SC_{01/12}$, respectively, with correlation factors larger than 0.95 (SL > 0.99). The fact that WMDW produced in 2005 corresponds to old WMDW characteristics in the CLXX simulations and to new WMDW in CTRL suggests that the exceptional atmospheric heat and salt losses that occurred during winter 2004–2005 were not responsible for the observed change of WMDW characteristics, and that this change was rather due to the evolution of the oceanic heat and salt contents until 2004.

[47] To investigate the contribution of the oceanic lateral fluxes of heat and salt during the convection to the characteristics of the WMDW formed in 2005, we perform heat and salt budgets over LION between $t_{\text{init}} = 1$ December 2004 and $t \leq t_{\text{fin}} = 31$ March 2005 for simulations performed under the atmospheric forcing of 2004–2005. During this period, the variation of heat content over LION is equal to the sum of the cumulated surface and lateral fluxes of heat, and the variation of salt content is equal to the cumulated lateral flux of salt:

$$\begin{aligned}\Delta_{t_{\text{init}}-t} HC &= \int_{t_{\text{init}}}^t HF_{\text{lat}}(t)dt + \int_{t_{\text{init}}}^t HF_{\text{surf}}(t)dt \\ \Delta_{t_{\text{init}}-t} SC &= \int_{t_{\text{init}}}^t SF_{\text{lat}}(t)dt\end{aligned}\quad (4)$$

[48] Note that surface freshwater flux associated to evaporation/precipitation (see section 2.2) does not appear in this equation. Indeed, freshwater flux does not modify the total salt content over the water column: there is no flux of salt through the ocean/atmosphere boundary, neither the water that evaporates nor the rainwater contain salt. However, surface freshwater flux induces a variation of the whole volume, and therefore a concentration/dilution that results in a modification of the average salinity. Rigorously, we should relate the salinity of DW to the average salinity over the water column rather than to the total salt content. The following scale analysis shows that this is equivalent.

[49] The variation of salinity induced by a change of volume dV due to evaporation/precipitation is equal to $dS_{WF} = -S_{\text{avg}}^{dV}/V$. The variation of salinity induced by a variation of salt content ΔSC is equal to $dS_{HC} = \frac{\Delta SC}{\rho V}$. Among winters examined in our sensitivity simulations, deep convection occurs during winters 1970–1971, 1980–1981 and 2004–2005. Between December and February, the net freshwater flux WF_{DJF} and the initial salt content on 1 December $SC_{01/12}$, in CTRL over the surface area are equal to $WF_{DJF} \sim 3.9 \text{ mm d}^{-1}$ and $SC_{01/12} \sim 8.729 \times 10^7 \text{ g m}^{-2}$, respectively, in 1970–1971, $WF_{DJF} \sim 3.6 \text{ mm d}^{-1}$ and $SC_{01/12} \sim 8.733 \times 10^7 \text{ g m}^{-2}$ in 1980–1981 and $WF_{DJF} \sim 4.4 \text{ mm d}^{-1}$ and $SC_{01/12} \sim 8.737 \times 10^7 \text{ g m}^{-2}$ in 2004–2005. Those values provide an estimate of the interannual variability of winter freshwater

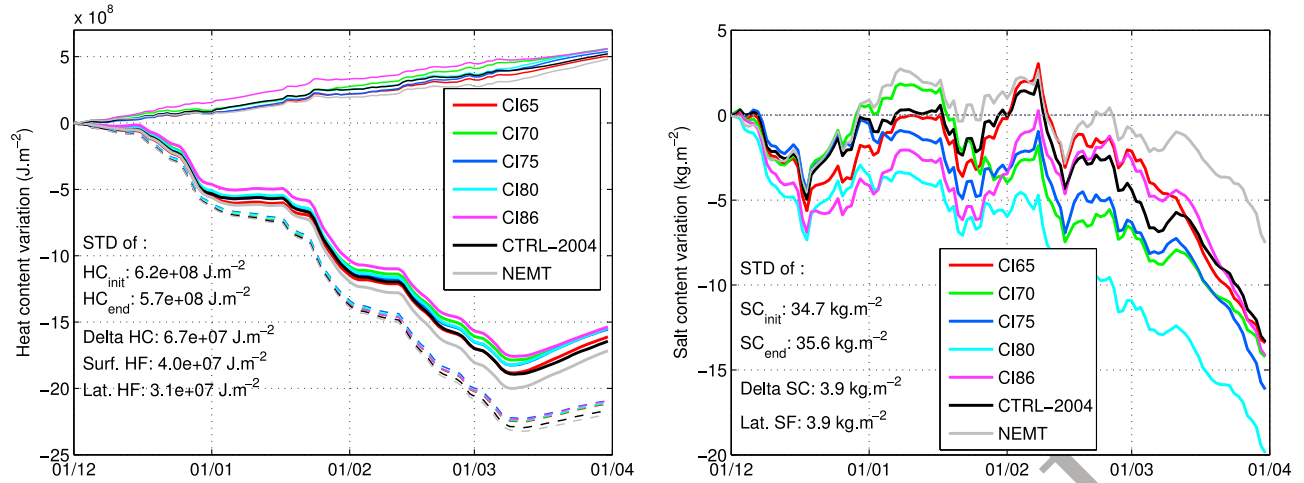


Figure 10. (left) Heat and (right) salt budgets over LION between December 2004 and March 2005 in the simulations performed under the atmospheric forcing of 2004–2005. Daily time series of the variation of the total heat and salt contents (HC and SC , bold lines), of the cumulated atmospheric heat flux (HF_{surf} , dashed lines), and of the cumulated lateral heat and salt fluxes (HF_{lat} and SF_{lat} , thin lines) since 1 December. Values of the initial contents on 1 December (HC_{init} , SC_{init}), of the final contents at the date of maximum convection, i.e., 10 March (HC_{fin} , SC_{fin}), of the variation of the heat content (Delta HC, Delta SC), of the cumulated surface heat flux (Surf. HC), and of the cumulated lateral atmospheric heat and salt fluxes (Lat. HC and Lat. SC) between 1 December and 10 March are indicated in black.

887 flux and initial salt content over years of deep convection.
 888 Between winters 1970–1971 or 1980–1981 and winter
 889 2004–2005, the difference of freshwater flux is $\Delta WF_{DJF} =$
 890 $[0.5; 0.8] \text{ mm d}^{-1}$ corresponding a difference of volume of
 891 $dV = [0.05; 0.08] \text{ m}$ over a period of 100 days (i.e., approxi-
 892 mately the length of the convection period, beginning of
 893 December to mid-March). The mean height of the water
 894 column is $\sim 2000 \text{ m}$. The difference of salinity induced by
 895 this difference of freshwater flux is therefore $dS_{WF} \sim 38 \times$
 896 $[0.05; 0.08]/2000 = [0.9; 1.5]10^{-3}$. Between winters 1970–
 897 1971 or 1980–1981 and winter 2004–2005, the difference of
 898 salt content is $\Delta SC_{01/12} = [40; 80]10^4 \text{ g m}^{-2}$. The difference
 899 of salinity induced by this difference of salt content is equal
 900 $dS_{SC} \sim [40; 80]10^4/(1029 \times 2000) = [1.9; 3.9]10^{-2}$.

901 [50] In our model, the variation of salinity induced by the
 902 interannual variability of freshwater fluxes during the con-
 903 vection period is therefore ~ 20 times smaller than the vari-
 904 ation of salinity associated to variability of the initial salt
 905 content, hence negligible. This justifies that we could
 906 neglect the impact of the freshwater flux on the average
 907 salinity and therefore relate the salinity of DW directly to the
 908 total salt content, and not only to the average salinity.

909 [51] The evolution of the terms of equation (4) are shown
 910 in Figure 10. The evolution of the variation of heat content
 911 during the convection event is very similar in each simula-
 912 tion, as well as the evolution of the cumulated lateral and
 913 surface heat fluxes. As a result, the contribution of those
 914 fluxes to the variability of the heat content is 1 order of
 915 magnitude smaller than the contribution of the initial heat
 916 content: the values of the standard deviation among the si-
 917 mulations of the total cumulated lateral and surface heat
 918 fluxes between 1 December and 10 March, when the con-
 919 vection is the strongest, are equal to $5 \cdot 10^7$ and $3 \cdot 10^7 \text{ J m}^{-2}$,
 920 respectively, i.e., approximately 10 to 20 times smaller than

the standard deviation of the initial heat content ($6 \cdot 10^8 \text{ J m}^{-2}$). Similarly, the variability of the lateral salt flux, which
 evolves similarly in each simulation, is much weaker than
 the variability of the initial salt content: the standard devi-
 ation of the total cumulated lateral salt flux is equal to 3.7 kg m^{-2} , i.e., ~ 10 times smaller than the standard deviation of
 the initial salt content (35 kg m^{-2}).

[52] Our results suggest that for given atmospheric con-
 ditions, the variability of the characteristics of the newly
 formed WMDW is mainly related to the variability of the
 initial heat and salt contents. The lateral oceanic heat and
 salt fluxes during the convection do not contribute signifi-
 cantly to the variability of these heat and salt contents, hence
 to the variability of the WMDW characteristics.

3.3.2.2. Impact of the Atmospheric Conditions During the 2004–2005 Convection Event on the WMDW Characteristics

[53] We showed in section 3.3.1 that the intensity of
 winter convection in terms of depth is mainly driven by the
 autumn and winter atmospheric conditions. The deeper the
 convection is, the larger the amount of WMDW already
 present in the convection area and mixed with the overlying
 water is. The relative proportions of WMDW and LIW
 contributing to the formation of new WMDW are therefore
 larger and smaller, respectively, when the convection is
 deeper. For given initial oceanic conditions, the WMDW
 being less warm and salty than the LIW, the temperature and
 salinity of the resulting newly formed WMDW will there-
 fore be smaller for larger depths of convection. This effect
 can be observed in our modeling study when comparing
 simulations where initial oceanic conditions are identical
 and where atmospheric conditions are different but induce
 deep convection, i.e., year 1970 of CTRL with CI70, year
 1980 of CTRL with CI80, and AF70, AF80 and year 2004

of CTRL: for given initial oceanic conditions, T_{DW} and S_{DW} decrease when MLD_{max} and MLD_{mean} increase (Table 3). In particular, the comparison of AF70, AF80 and year 2004 of CTRL shows that if different atmospheric conditions had occurred in 2004–2005, e.g., those of winters 1970–1971 or 1980–1981, deep convection could still have occurred ($MLD_{max} = 1883$ m in AF70, 2562 m in AF80 and 2601 m in CTRL) and the change of WMDW could have been even more spectacular than the change observed in reality since the mixed layer would have been slightly shallower (T_{DW} and S_{DW} are equal to 13.04°C and 38.513 in AF70 and 12.92°C, 38.488 in AF80 versus 12.90°C, 38.483 in CTRL). Another interesting point is that the characteristics of convection during winter 1980–1981 of CTRL (12.90°C, 38.479 and 29.113 kg m⁻³) correspond to new characteristics: the conjunction of smaller heat and salt contents than those of August 2004 (1.188 10¹¹ J m⁻² and 8.733 10⁴ kg m⁻² in 1980–1981 versus 1.198 10¹¹ J m⁻² and 8.737 10⁴ kg m⁻² in 2004–2005; Figure 4 and Table 3) with smaller maximum and mean MLD (2382 m and 510 m versus 2601 m and 943 m; Table 3) led to the formation of WMDW with similar characteristics (12.90°C, 38.479 versus 12.90°C, 38.483). Finally the atmospheric conditions during the convection indirectly influence the characteristics of newly formed WMDW by determining the depth of convection.

3.3.2.3. Impact of the EMT on WMDW Characteristics

[54] Finally, the results obtained in sections 3.3.2.2 and 3.3.2.1 show that the change of temperature and salinity of the WMDW formed during winter 2004–2005 compared to the WMDW formed before was not due to the atmospheric conditions neither to the lateral oceanic advection during this winter, but to the initial heat and salt contents of autumn 2004 over LION, which were exceptionally high. We showed in section 3.1 that these high 2004 contents, obtained both in NEMT and CTRL, were not due to the EMT but to the absence of deep convection during the 1990s, itself induced by a succession of weak buoyancy loss winters. Our results therefore show that the EMT was not responsible for the change of WMDW characteristics observed during the 2005 convection episode, contrary to what was suggested by *Schroeder et al.* [2008].

[55] Note that this result explains why the simulation used by *Herrmann et al.* [2009] in order to study the interannual variability of the NWMD convection for the period 1998–2007 was not able to reproduce the change of WMDW characteristics observed in 2005. During the 10 years spin-up corresponding to the period 1987–1997, ERA40 fields were indeed used for the atmospheric forcing. Their resolution, ~125 km, is not sufficient to reproduce realistically the Mediterranean circulation and in particular the NWMD deep convection [*Herrmann and Somot*, 2008]. Consequently, this simulation could not reproduce correctly the circulation of water masses during this period in the NWMD, and therefore the salting and warming responsible for the change of WMDW characteristics observed in 2005.

4. Conclusion

[56] In this paper we focus on the exceptionally strong convection event that occurred in the NWMD during winter 2004–2005, associated with newly formed WMDW warmer and saltier than usually. Experimental oceanographers that

observed this event proposed two explanations: the first one relates the exceptional intensity of this convection event, as well as the change of the characteristics of WMDW formed this winter to the atmospheric conditions. The second one relates them to the effect of the EMT on the intermediate layer of the NWMD, hence on the oceanic conditions. We used numerical modeling in order to determine which element played a role in this event, and how.

[57] We first performed a realistic numerical simulation of the Mediterranean oceanic circulation during the 1960–2006 period. The long-term analysis of this simulation was performed by *Beuvier et al.* [2010], who validated the long-term evolution of the temperature and salinity in the whole basin, and showed that the model reproduces correctly the EMT. Here we showed that this control simulation is able to reproduce realistically the 2005 NWMD convection event: the temporal and spatial evolution of the convection event as well as the WMDW characteristics were consistent with satellite and in situ observations.

[58] Sensitivity simulations then allowed us to assess the respective contributions of the oceanic and atmospheric conditions to the 2004–2005 convection event. First, we examined the factors that led to the structure of the water column in the NWMD just before the convection. Our model suggests that a succession of winters of weak atmospheric buoyancy loss was responsible for the absence of deep convection during the 1990s. This would have enabled the heat and salt to accumulate in the intermediate layer. Consequently, the heat and salt contents of autumn 2004 were the highest of the whole 1960–2005 period, in agreement with the observations of *Schroeder et al.* [2010]. According to our model, the EMT did not contribute significantly to this warming and salting of the intermediate layer, but it induced the deepening of the heat and salt maximum in the NWMD. This deepening, already observed by *Gasparini et al.* [2005], was associated with a weakening of the stratification of the water column in autumn 2004 compared to what would have been the case without the EMT.

[59] We then determined which were the key factors that could be responsible for the characteristics of the 2004–2005 convection event. In our model, the abrupt change of WMDW characteristics observed in 2005 predominantly resulted from the high heat and salt contents of autumn 2004. It therefore seems that it was not due to the EMT but to the weakness of the winter atmospheric buoyancy loss and deep convection in the NWMD during the 1990s. Moreover, our results suggest that the lateral oceanic heat and salt fluxes during winter 2004–2005 did not play a significant role in the settings of the WMDW characteristics. The atmospheric conditions of 2004–2005, namely the strong autumn and winter atmospheric buoyancy losses, mainly drove the deepening of the mixed layer in our model. They consequently appear to be the major factor responsible for the exceptional intensity of the convection observed this winter in terms of depth and volume of newly formed WMDW. The EMT would have accentuated the effect of the atmospheric forcing by weakening the stratification, hence facilitating the vertical mixing of the water column. This would have not fundamentally change the convection process and depth but potentially doubled the volume of newly formed WMDW. Finally, our conclusions were obtained using a given ocean model forced by a given atmospheric

data set. It would be necessary to perform other simulations using other models and atmospheric forcings in order to enforce the robustness of our conclusions or to propose alternative explanations.

[60] In this study, we focused on winter 2004–2005 and on the NWMED in order to understand the mechanisms responsible for the spectacular convection that occurred this year. WMDW formed in 2005 then propagated into the rest of the basin [Schroeder et al., 2008] and a signal apparently reached the Gibraltar Strait. García Lafuente et al. [2007] indeed observed a decrease of the temperature of the Mediterranean Outflow Water in March 2005 and 2006. They attributed it to a remote signature of the strong NWMED convection that occurred those winters. Our simulations could help to understand how the 2004–2005 convection event in the NWMED influenced the circulation in the rest of the basin and this motivates further studies. Our next goal is to use and perform additional realistic long-term simulations in order to quantify more generally the contributions of the oceanic and atmospheric conditions to the interannual variability of the convection characteristics, in the NWMED but also in the other regions of deep and intermediate convection of the Mediterranean Sea (Adriatic, Aegean, Levantine subbasins) and study how these local processes can interact between each other in particular through the thermohaline circulation.

[61] **Acknowledgments.** This study has been sponsored by the “Forecast and projection in climate scenario of Mediterranean intense events: Uncertainties and Propagation on environment” (MEDUP) project of the program Vulnérabilité: Milieux et Climat from the Agence Nationale pour la Recherche and by the HyMeX project (Hydrological cycle in the Mediterranean experiment (www.hymex.org)). We thank C. Millot, K. Schroeder, and an anonymous reviewer for their comments and suggestions that helped to improve the quality of this paper. We also thank D. Quoc-Phi, M. Remaud, and A. Verrelle for their work at the very beginning of this study.

References

- Barnier, B., et al. (2006), Impact of partial steps and momentum advection schemes in a global ocean circulation model at eddy-permitting resolution, *Ocean Dyn.*, **56**, 543–567.
- Beuvier, J., F. Sevault, M. Herrmann, H. Kontoyiannis, W. Ludwig, M. Rixen, E. Stanev, K. Béranger, and S. Somot (2010), Modeling the Mediterranean Sea interannual variability during 1961–2000: Focus on the Eastern Mediterranean Transient (EMT), *J. Geophys. Res.*, **115**, C08017, doi:10.1029/2009JC005950.
- Blanke, B., and P. Delecluse (1993), Variability of the tropical Atlantic Ocean simulated by a general circulation model with two different mixed layer physics, *J. Phys. Oceanogr.*, **23**, 1363–1388.
- Bozec, A., P. Bouret-Aubertot, D. Iudicone, and M. Crépon (2008), Impact of penetrative solar radiation on the diagnosis of water mass transformation in the Mediterranean Sea, *J. Geophys. Res.*, **113**, C06012, doi:10.1029/2007JC004606.
- Castellari, S., N. Pinardi, and K. Leaman (2000), Simulation of water mass formation processes in the Mediterranean Sea: Influence of the time frequency of the atmospheric forcing, *J. Geophys. Res.*, **105**(C10), 24,157–24,181, doi:10.1029/2000JC900055.
- CLIPPER Project Team (1999), Modélisation à haute résolution de la circulation dans l’océan Atlantique forcée et couplée océan-atmosphère, *Sci. Tech. Rep. CLIPPER-R3-99*, Lab. des Ecoulements Géophys. et Ind., Grenoble, France.
- Déqué, M., and J. Piedelievre (1995), High-resolution climate simulation over Europe, *Clim. Dyn.*, **11**, 321–339.
- Font, J., P. Puig, J. Salat, A. Palanques, and M. Emelianov (2007), Sequence of hydrographic changes in NW Mediterranean deep water due to the exceptional winter of 2005, *Sci. Mar.*, **71**, 339–346.
- García Lafuente, J., A. Sánchez Román, G. Díaz del Río, G. Sannino, and J. C. Sánchez Garrido (2007), Recent observations of seasonal variability of the Mediterranean outflow in the Strait of Gibraltar, *J. Geophys. Res.*, **112**, C10005, doi:10.1029/2006JC003992.
- Gasparini, G., A. Ortona, G. Budillon, M. Astraldi, and E. Sansone (2005), The effect of the Eastern Mediterranean Transient on the hydrographic characteristics in the Strait of Sicily and in the Tyrrhenian Sea, *Deep Sea Res., Part II*, **52**, 915–935.
- Gibson, J., P. Kållberg, S. Uppala, A. Hernandez, and E. Serano (1997), ERA description, in *Re-anal. Proj. Rep. Ser.*, Eur. Cent. for Medium-Range Weather Forecast, Reading, U. K.
- Guldborg, A., E. Kaas, M. Déqué, S. Yang, and S. Vester Thorsen (2005), Reduction of systematic errors by empirical model correction: Impact on seasonal prediction skill, *Tellus, Ser. A*, **57**, 575–588.
- Herrmann, M. J., and S. Somot (2008), Relevance of ERA40 dynamical downscaling for modeling deep convection in the Mediterranean Sea, *Geophys. Res. Lett.*, **35**, L04607, doi:10.1029/2007GL032442.
- Herrmann, M., S. Somot, F. Sevault, C. Estournel, and M. Déqué (2008), Modeling the deep convection in the northwestern Mediterranean sea using an eddy-permitting and an eddy-resolving model: Case study of winter 1986–1987, *J. Geophys. Res.*, **113**, C04011, doi:10.1029/2006JC003991.
- Herrmann, M., J. Bouffard, and K. Béranger (2009), Monitoring open-ocean deep convection from space, *Geophys. Res. Lett.*, **36**, L03606, doi:10.1029/2008GL036422.
- Kalnay, E., et al. (1996), The NCEP/NCAR 40-year reanalysis project, *Bull. Am. Meteorol. Soc.*, **77**, 437–471.
- López-Jurado, J.-L., C. González-Pola, and P. Vélaz-Belchí (2005), Observation of an abrupt disruption of the long-term warming trend at the Balearic Sea, western Mediterranean Sea, in summer 2005, *Geophys. Res. Lett.*, **32**, L24606, doi:10.1029/2005GRL024430.
- Madec, G. (2008), NEMO ocean engine, *Note Pole de Modélisation 27*, Inst. Pierre-Simon Laplace, Paris.
- Marshall, J., and F. Schott (1999), Open-ocean convection: Observations, theory, and models, *Rev. Geophys.*, **37**(1), 1–64.
- MEDAR/MEDATLAS Group (2002), *MEDAR/MEDATLAS 2002 Database: Cruise Inventory, Observed and Analysed Data of Temperature and Bio-Chemical Parameters* [4 CD-ROMs], Inst. Fr. de Rech. Pour l’Exploit. de la Mer, Brest, France.
- Mertens, C., and F. Schott (1998), Interannual variability of deep-water formation in the northwestern Mediterranean, *J. Phys. Oceanogr.*, **28**, 1410–1424.
- Millot, C. (1999), Circulation in the western Mediterranean Sea, *J. Mar. Syst.*, **20**, 423–442.
- Millot, C. (2005), Circulation in the Mediterranean Sea: Evidences, debates and unanswered questions, *Sci. Mar.*, **69** 5–21, doi:10.3989/scimar.2005.69s15.
- Perry, K. (2001), SeaWinds on QuikSCAT Level 3 Daily, Gridded Ocean Wind Vectors (JPL SeaWinds Project), http://podaac.jpl.nasa.gov/DATA_CATALOG/quikscatinfo.html, JPL Phys. Oceanogr. DAAC, Pasadena, Calif.
- Reynaud, T., P. Legrand, H. Mercier, and B. Barnier (1998), A new analysis of hydrographic data in the Atlantic and its application to an inverse modeling study, *Int. World Ocean Circ. Exp. Newsl.* **32**, Natl. Oceanogr. Data Cent., Silver Spring, Md.
- Rixen, M., et al. (2005), The Eastern Mediterranean Deep Water: A proxy for climate change, *Geophys. Res. Lett.*, **32**, L12608, doi:10.1029/2005GL022702.
- Roether, W., B. Klein, B. Manca, A. Theocharis, and S. Kioroglou (2007), Transient eastern Mediterranean deep waters in response to the massive dense-water output of the Aegean Sea in the 1990s, *Prog. Oceanogr.*, **74**, 540–571.
- Salat, J., M. Emelianov, and J. López-Jurado (2006), Unusual extension of western Mediterranean deep water formation during winter 2005, paper presented at 5 Asamblea Hispano-Portuguesa de Geodesia y Geofísica, Minist. de Medio Ambiente, Sevilla, Spain.
- Sannino, G., M. Herrmann, A. Carillo, V. Rupolo, V. Ruggiero, V. Artale, and P. Heimbach (2009), An eddy-permitting model of the Mediterranean Sea with a two-way grid refinement at the Strait of Gibraltar, *Ocean Modell.*, **30**, 56–72, doi:10.1016/j.ocemod.2009.06.002.
- Schröder, K., G. P. Gasparini, M. Tangherlini, and M. Astraldi (2006), Deep and intermediate water in the western Mediterranean under the influence of the Eastern Mediterranean Transient, *Geophys. Res. Lett.*, **33**, L21607, doi:10.1029/2006GL027121.
- Schroeder, K., A. Ribotti, M. Borghini, R. Sorgente, A. Perilli, and G. P. Gasparini (2008), An extensive Western Mediterranean Deep Water renewal between 2004 and 2006, *Geophys. Res. Lett.*, **35**, L18605, doi:10.1029/2008GL035146.
- Schroeder, K., S. A. Josey, M. Herrmann, L. Grignon, G. P. Gasparini, and H. L. Bryden (2010), Abrupt warming and salting of the Western Med-

- 1222 iterranean Deep Water: Atmospheric forcings and lateral advection, 1237
 1223 *J. Geophys. Res.*, *115*, C08029, doi:10.1029/2009JC005749. 1238
 1224 Sevault, F., S. Somot, and J. Beuvier (2009), A regional version of the 1239
 1225 NEMO ocean engine on the Mediterranean Sea: NEMOMED8 user's 1240
 1226 guide, *Note Cent. 107*, Groupe de Météorol. de Grande Echelle et Climat, 1241
 1227 CNRM, Toulouse, France. 1242
 1228 Smith, R. O., H. L. Bryden, and K. Stansfield (2008), Observations of new 1243
 1229 Western Mediterranean Deep Water formation using Argo floats 2004– 1244
 1230 2006, *Ocean Sci.*, *4*, 133–149. 1245
 1231 Smith, W., and D. Sandwell (1997), Global sea floor topography from sat-
 1232 ellite altimetry and ship depth sounding, *Science*, *277*(5334), 1956–1962.
 1233 Somot, S., F. Sevault, and M. Déqué (2006), Transient climate change sce-
 1234 nario simulation of the Mediterranean Sea for the twenty-first century
 1235 using a high-resolution ocean circulation model, *Clim. Dyn.*, *27*, 851–
 1236 579, doi:10.1007/s00382-006-0167-z.
- Stanev, E., P.-Y. Le Traon, and E. Peneva (2000), Sea level variations and
 their dependency on meteorological and hydrological forcing: Analysis
 of altimeter and surface data for the Black Sea, *J. Geophys. Res.*,
105(C7), 17,203–17,216.
 Testor, P., and J.-C. Gascard (2006), Post-convection spreading phase in
 the northwestern Mediterranean Sea, *Deep Sea Res., Part I*, *53*, 869–893.
 Vörösmarty, C., B. Fekete, and B. Tucker (1996), *Global River Discharge*
Database (RivDis), *Int. Hydrol. Program*, Global Hydrol. Archive and
 Anal. Syst., UNESCO, Paris.
- J. Beuvier, ENSTA-ParisTech/UME, Chemin de la Hunière, F-91761
 Palaiseau CEDEX, France.
 M. Herrmann, F. Sevault, and S. Somot, CNRM-GAME, Météo-France,
 42 Ave. Gaspard Coriolis, F-31057 Toulouse CEDEX, France. (marine.
 herrmann@m4x.org)

Article in Proof